PLOS PATHOGENS

RESEARCH ARTICLE

Exclusive dependence of IL-10Rα signalling on intestinal microbiota homeostasis and control of whipworm infection

María A. Duque-Correa[1]*, Natasha A. Karp[1¤], Catherine McCarthy[1], Simon Forman[2], David Goulding[1], Geetha Sankaranarayanan[1], Timothy P. Jenkins[3], Adam J. Reid[1], Emma L. Cambridge[1], Carmen Ballesteros Reviriego[1], The Sanger Mouse Genetics Project[1], The 3i consortium, Werner Müller[4], Cinzia Cantacessi[3], Gordon Dougan[1], Richard K. Grencis[2], Matthew Berriman[1]

1 Wellcome Sanger Institute, Wellcome Genome Campus, Hinxton, United Kingdom, **2** Lydia Becker Institute of Immunology and Inflammation, Wellcome Trust Centre for Cell Matrix Research and Faculty of Biology, Medicine and Health, University of Manchester, Manchester, United Kingdom, **3** Department of Veterinary Medicine, University of Cambridge, Cambridge, United Kingdom, **4** Lydia Becker Institute of Immunology and Inflammation and Faculty of Biology, Medicine and Health, University of Manchester, Manchester, United Kingdom

¤ Current address: Quantitative Biology, Discovery Sciences, IMED Biotech Unit, AstraZeneca, Cambridge, United Kingdom.
* md19@sanger.ac.uk

Citation: Duque-Correa MA, Karp NA, McCarthy C, Forman S, Goulding D, Sankaranarayanan G, et al. (2019) Exclusive dependence of IL-10Rα signalling on intestinal microbiota homeostasis and control of whipworm infection. PLoS Pathog 15(1): e1007265. https://doi.org/10.1371/journal.ppat.1007265

Editor: Nicola Harris, Monash University, AUSTRALIA

Received: August 2, 2018

Accepted: December 4, 2018

Published: January 14, 2019

Data Availability Statement: All sequencing reads for 16S microbiota analysis are available from the ENA database (www.ebi.ac.uk/ena) (accession numbers ERP016361).

Funding: MADC has received funding from the European Union's Horizon 2020 research and innovation programme under the Marie Sklodowska-Curie grant agreement No 656347 (www.ec.europa.eu/research/mariecurieactions/). The 3i consortium was supported by Wellcome

Abstract

The whipworm *Trichuris trichiura* is a soil-transmitted helminth that dwells in the epithelium of the caecum and proximal colon of their hosts causing the human disease, trichuriasis. Trichuriasis is characterized by colitis attributed to the inflammatory response elicited by the parasite while tunnelling through intestinal epithelial cells (IECs). The IL-10 family of receptors, comprising combinations of subunits IL-10Rα, IL-10Rβ, IL-22Rα and IL-28Rα, modulates intestinal inflammatory responses. Here we carefully dissected the role of these subunits in the resistance of mice to infection with *T. muris*, a mouse model of the human whipworm *T. trichiura*. Our findings demonstrate that whilst IL-22Rα and IL-28Rα are dispensable in the host response to whipworms, IL-10 signalling through IL-10Rα and IL-10Rβ is essential to control caecal pathology, worm expulsion and survival during *T. muris* infections. We show that deficiency of IL-10, IL-10Rα and IL-10Rβ results in dysbiosis of the caecal microbiota characterised by expanded populations of opportunistic bacteria of the families *Enterococcaceae* and *Enterobacteriaceae*. Moreover, breakdown of the epithelial barrier after whipworm infection in IL-10, IL-10Rα and IL-10Rβ-deficient mice, allows the translocation of these opportunistic pathogens or their excretory products to the liver causing organ failure and lethal disease. Importantly, bone marrow chimera experiments indicate that signalling through IL-10Rα and IL-10Rβ in haematopoietic cells, but not IECs, is crucial to control worm expulsion and immunopathology. These findings are supported by worm expulsion upon infection of conditional mutant mice for the IL-10Rα on IECs. Our findings emphasize the pivotal and complex role of systemic IL-10Rα signalling on immune cells in promoting microbiota homeostasis and maintaining the intestinal epithelial barrier, thus preventing immunopathology during whipworm infections.

Trust grant [100156] (www.immunophenotype.org). The funders had no role in study design, data collection and analysis, decision to publish, or preparation of the manuscript.

Competing interests: The authors have declared that no competing interests exist.

Author summary

The human gut is home to millions of bacteria, collectively called the microbiota, and also to parasites that include whipworms. The interactions between gut cells, the microbiota and whipworms define conditions for balanced parasitism. Cells lining the gut host whipworms but also interact with gut immune cells to deploy measures that control or expel whipworms whilst maintaining a barrier to prevent microbial translocation. Whipworms affect the composition of the microbiota, which in turn impacts the condition of the gut lining and the way in which immune cells are activated. In order to avoid tissue damage and disease, these interactions are tightly regulated. Here we show that signalling through a member of the IL-10 receptor family, IL-10Rα, in gut immune cells is critical for regulating of these interactions. Lack of this receptor on gut immune cells results in persistence of whipworms in the gut accompanied by an uncontrolled inflammation that destroys the gut lining. This tissue damage is accompanied by the overgrowth of members of the microbiota that act as opportunistic pathogens. Furthermore, the destruction of the gut barrier allows these bacteria to reach the liver where they cause organ failure and fatal disease.

Introduction

A single layer of intestinal epithelial cells (IECs) in conjunction with the overlaying mucus acts as a primary barrier to viruses, bacteria and parasites entering the body via the gastrointestinal tract [1]. Paradoxically, the intestinal epithelium is also the host tissue for diverse pathogens including intestinal parasitic worms [2, 3]. Amongst the intestinal worms, whipworms (*Trichuris trichiura*) infect hundreds of millions of people and cause trichuriasis, a major Neglected Tropical Disease [4, 5].

Whipworms live preferentially in the caecum of their host, where they tunnel through IECs and cause inflammation that potentially results in colitis [6, 7]. It has been proposed that IEC activation, resulting from the initial recognition or physical contact with whipworms, influences the immunological response that ultimately determines whether parasites are expelled from the intestine or persist embedded in the intestinal epithelium causing a chronic disease [2, 4]. Most of our understanding of the host response to whipworms comes from studies of the natural whipworm infection of mice with *T. muris*, which closely mirrors that of humans [3, 7]. Resistance to infection is recapitulated by infecting mice with a high dose (200–400) of *T. muris* eggs and is mediated by a type-2 immune response that includes increased production of interleukin 4 (IL-4), IL-13, IL-25, IL-33, IL-9 and antibody isotypes IgG1 and IgE and results in worm expulsion [3, 7]. Conversely, chronic disease is modelled by infecting mice with a low dose (20–25) of *T. muris* eggs that results in the development of a type-1 immune response characterised by production of inflammatory cytokines, mainly IFN-γ, and the antibody isotype IgG2a/c [3, 7]. Type-1 immunity promotes intestinal inflammation that when severe can cause colitis [3, 7]. However, in chronic infections such responses are modulated by the parasite to optimize their residence and reproduction and ensure host survival, thus achieving a balanced parasitism [4, 7]. This immunomodulation is partly mediated by transforming growth factor (TGF)-β, IL-35 and IL-10 production by macrophages and T cells in response to excretory-secretory (ES) parasite antigens [3, 4, 7]. Besides this immunomodulatory role of IL-10 in chronic infections, IL-10 is important in the induction of host resistance (through type-2 response) during acute (high dose) *T. muris* infections [3, 8].

Intestinal mucosal homeostasis is regulated principally through IL-10 receptor signalling [9]. The IL-10 receptor is a heterotetramer complex composed of two alpha and two beta subunits, IL-10Rα and IL-10Rβ, respectively [9, 10]. While the IL-10Rα subunit is unique to IL-10, the IL-10Rβ chain is shared by receptors for other members of the IL-10 superfamily of cytokines [9–12]. Specifically, a single IL-10Rβ subunit pairs with IL-22Rα, IL-20Rα, or IL-28Rα subunits to form the receptors for IL-22, IL-26 and the interferon λ species (IL-28α, IL-28β and IL-29), respectively [10–12] *(S1 Fig)*.

IL-10 is a key anti-inflammatory cytokine that limits innate and adaptive immune responses [9, 10]. The development of spontaneous enterocolitis in mice deficient for IL-10 and IL-10Rβ has demonstrated the crucial role of IL-10 in maintaining the integrity of the intestinal epithelium [13, 14]. Similarly, IL-22 contributes to the homeostasis of mucosal barriers by directly mediating epithelial defence mechanisms that include inducing the production of antimicrobial peptides, selected chemokines and mucus. IL-22 is also involved in tissue protection and regeneration [10, 12, 15]. The IL-22 receptor is exclusively expressed on non-haematopoietic cells, such as IECs [10, 12, 15]. Likewise, IL-28 receptor expression is largely restricted to cells of epithelial origin, although also expressed in B cells, macrophages and plasmacytoid DCs, where it mediates the antiviral, antitumor and potentially antibacterial functions of the interferon λ species [10, 16–18]. IL-26 is also reported to promote defence mechanisms against viruses and bacteria at mucosal surfaces in humans, however, the IL-26 receptor in the mouse is an orphan receptor because the *Il-26* gene locus is not present in mice [10, 11, 19].

Previous studies indicate the importance of the IL-10 receptor signalling in responses to whipworms. Specifically, IL-10 promotes host resistance and survival to whipworm infection, with IL-10 deficiency leading to morbidity and mortality that may be due to a breakdown of the epithelial barrier and the outgrowth of opportunistic bacteria [8, 20]. Mice lacking the IL-10Rα chain develop a chronic *T. muris* infection accompanied by intestinal inflammation [21]. Furthermore, in IL-22-deficient mice whipworm expulsion is delayed, correlating with reduced goblet cell hyperplasia [22]. However, the specific role that each subunit (IL-10Rα, IL-10Rβ, IL-22Rα and IL-28Rα) plays on the intestinal epithelia barrier maintenance, mucosal homeostasis and broader host response to this parasite remains unclear. There is also little understanding on how these receptors can promote resistance to colonisation by opportunistic members of the microbiota that potentially drive the pathology observed in the absence of IL-10 during whipworm infection.

In the present study, we use mutant mice to dissect the role of IL-10Rα, IL-10Rβ, IL-22Rα and IL-28Rα in host resistance to *T. muris* infections. We demonstrate that IL-10 signalling, exclusively through IL-10Rα and IL-10Rβ, promotes resistance to colonization by intestinal opportunistic bacterial pathogens and maintenance of the intestinal epithelial barrier, thus preventing the development of systemic immunopathology during whipworm infection.

Materials and methods

Ethics statement

The care and use of mice were in accordance with the UK Home Office regulations (UK Animals Scientific Procedures Act 1986) under the Project licenses 80/2596 and P77E8A062 and were approved by the institutional Animal Welfare and Ethical Review Body. All efforts were made to minimize suffering by considerate housing and husbandry. Animal welfare was assessed routinely for all mice involved. Mice were naïve prior the studies here described.

Mice

Il10$^{-/-}$ *and Il10ra*$^{-/-}$ mice in a C57BL/6J background were obtained by treatment of *Il10*$^{fl/fl}$ *and Il10ra*$^{fl/fl}$ [21] embryos with *cre* recombinase. *Il10ra*$^{fl/fl}$ *Vil*$^{cre/+}$ mice were obtained by crossing of *Il10ra*$^{fl/fl}$ with *Vil*$^{cre/+}$ *mice*. *Il22*$^{-/-}$ mice, as previously described [23], were received from Prof. Fiona Powrie (University of Oxford).

Il10rb$^{tm1b/tm1b}$, *Il22ra1*$^{tm1a/tm1a}$, *Ifnlr1*$^{tm1a/tm1a}$, *Rag1*^{tm1Mom} and wild-type (WT) C57BL/6N mice were maintained and phenotyped by the Sanger Mouse Genetics Programme [24]. For experiments with *Il10*$^{-/-}$, *Il10ra*$^{-/-}$, *Il10rb*$^{tm1b/tm1b}$ and *Il10ra*$^{fl/fl}$ *Vil*$^{cre/+}$ colonies, both WT and mutant mice littermates were derived from heterozygous breeding pairs. All animals were kept under specific pathogen-free conditions, and colony sentinels tested negative for *Helicobacter* spp. Mice were fed a regular autoclaved chow diet (LabDiet) and had *ad libitum* access to food and water.

Bone marrow chimeras

Recipient mice were irradiated with two 5-Gy doses, 4 h apart, and injected intravenously with bone marrow harvested from donor mice at 2 million cells per 200 μl sterile phosphate-buffered saline. The mice were transiently maintained on neomycin sulfate (100mg/L, Cayman Chemical) in their drinking water for 2 weeks (wk). Bone marrow was allowed to reconstitute for 4 wk before mice were infected with *T*. *muris*.

Parasites and *T*. *muris* infection

Infection and maintenance of *T*. *muris* was conducted as described [25]. Age and sex matched female and male WT and mutant mice (6–10 wk old) were orally infected under anaesthesia with isoflurane with a high (400) or low (20–25) dose of embryonated eggs from *T*. *muris* E-isolate. Mice were randomised into uninfected and infected groups using the Graph Pad Prism randomization tool. Uninfected and infected mice were co-housed. Mice were monitored daily for general condition and weight loss. Mice were culled including concomitant controls (uninfected and WT mice) at different time points or when their condition deteriorated (observation of hunching, piloerection, reduced activity or weight loss from body weight at the beginning of infection reaching 20%). Mice were killed by terminal anesthesia followed by exsanguination and cervical dislocation. The worm burden was blindly assessed by counting larvae that were present in the caecum. Blinding at the point of measurement was achieved by the use of barcodes. During sample collection, group membership could be seen, however this stage was completed by technician staff with no knowledge of the experiment objectives.

IL-10Rα blocking by antibody treatment

Every other day, from day 35 to day 45 p.i., whipworm-infected *Rag1*^{tm1Mom} mice were intraperitoneally injected with an antibody blocking the IL-10Rα (BioXcell, clone 1B1.3A) or an isotype control (BioXcell, clone HRPN) for a total delivery of 2mg per mouse.

Parasite atigen

Adult worms were cultured in RPMI 1640 (Sigma-Aldrich) and ES products were collected after 4 h and following overnight culture. The ES were prepared as described [26].

Histology

To evaluate disease pathology, caecal and liver segments were fixed in 4% paraformaldehyde and 2–5 μm paraffin sections were stained in haematoxylin and eosin (H&E) or Periodic Acid-

Schiff (PAS) according to standard protocol. Slides were scanned using a Hamamatsu NanoZoomer 2.0HT digital slide scanner (Meyer Instruments, Inc) and images were analysed using the NDP View2 software. From blinded and randomised histological slides, intestinal inflammation was scored by two research assistants as follows: submucosal and mucosal oedema (0, absent; 1, mild; 2, moderate; or 3, severe); submucosal and mucosal inflammation (0, absent; 1, mild; 2, moderate; or 3, severe); percentage of area involved (0, 0–5%; 1, mild, 10–25%; 2, moderate, 30–60%; or 3, severe, >70%). Crypt lengths were measured and goblet cells counted. Liver pathology was documented, including presence of immune infiltrate, granulomas and necrosis.

For immunofluorescence, 5 μm sections of frozen caecal and liver tissues were stained with α-*Enterococcus* spp. antibody (1/1000, LSBio), α-*Escherichia coli* spp. antibody (1/1000, LSBio) or α-ZO-1 (1/200 ThermoScientific). Sections were mounted using ProLong Gold anti-fade reagent (Molecular Probes) containing 4',6'-diamidino-2-phenylindole (DAPI) for nuclear staining. Confocal microscopy images were taken with a Leica SP8 confocal microscope. From each mouse, a slide was examined to determine the presence of bacterial infection in the liver. Although only low sensitivity is possible from a single slide per mouse, bacteria should not be present in the livers of healthy animals, and any detected therefore indicate bacterial translocation.

For transmission electron microscopy, tissues were fixed in 2.5% glutaraldehyde/2% paraformaldehyde, post-fixed with 1% osmium tetroxide in 0.1M sodium cacodylate buffer and mordanted with 1% tannic acid followed by dehydration through an ethanol series (contrasting with uranyl acetate at the 30% stage) and embedding with an Epoxy Resin Kit (Sigma-Aldrich). Ultrathin sections cut on a Leica UC6 ultramicrotome were contrasted with uranyl acetate and lead nitrate, and images recorded on a FEI 120 kV Spirit Biotwin microscope on an F415 Tietz CCD camera.

Specific antibody ELISA

Levels of parasite-specific immunoglobulins IgG1 and IgG2a/c were determined by ELISA in serum as described [27]. Briefly, ELISA plates (Nunc Maxisorp, Thermo Scientific) were coated with 5 μg/ml *T. muris* overnight-ES. Serum was diluted from 1/20 to 1/2560, and parasite-specific IgG1 and IgG2a/c were detected with biotinylated anti-mouse IgG1 (Biorad) and biotinylated anti-mouse IgG2a/c (BD PharMingen), respectively.

IL-6 and TNF-α ELISA

Serum IL-6 and TNF-α were determined with the Mouse IL-6 and TNF-α ReadySet-Go! ELISA kits (eBioscience).

Limulus amebocyte lysate (LAL) assay

The presence of lipopolysaccharide (LPS) in serum was determined with the LAL assay kit (Hycult Biotech).

Plasma chemistry analysis

Blood was collected under terminal anaesthesia into heparinized tubes for plasma preparation. Within 1 hour of collection, blood samples were centrifuged and plasma recovered and stored at -20˚C until analysis. Clinical chemistry analysis of plasma was performed using the Olympus AU400 analyzer (Beckman Coulter Ltd) and was blinded to the operator via barcodes.

The majority of parameters were measured using kits and controls supplied by Beckman Coulter. Samples were also tested for haemolysis. Four parameters were measured by kits not supplied by Beckman Coulter: transferrin, ferritin (Randox Laboratories Ltd), fructosamine (Roche Diagnostic) and thyroxine (Thermo Fisher).

16S rRNA-based identification of bacterial species

To identify microbial species from the livers of mice, mouse tissues were homogenized aseptically under laminar flow. Organ lysates were immediately cultured in nonselective Luria-Bertani (LB) and Brain Heart Infusion (BHI) media under aerobic and anaerobic conditions for 36–48 h. All colonies from each plate, or within a defined section, were picked in an unbiased manner for DNA extraction and 16S rRNA gene sequencing using the universal primers: 7F, 50-AGAGTTTGATYMTGGCTCAG-30; 926R, 50-ACTCCTACGGGAGGCAGCAG-30. Bacterial identifications were performed using the 16S rRNA NCBI Database for Bacteria and Archaea.

Microbiota analysis

To study the caecal and liver microbiota composition of uninfected and *T. muris*-infected mice, luminal contents of the caecum were collected by manual extrusion and a piece of liver was taken upon culling of mice. Bacterial DNA was obtained using the FastDNA Spin Kit for Soil (MBio) and FastPrep Instrument (MPBiomedicals). V5-V3 regions of bacterial 16S rRNA genes were PCR amplified with high-fidelity AccuPrime Taq Polymerase (Invitrogen) and primers: 338F, 50-CCGTCAATTCMTTTRAGT-30; 926R, 50-ACTCCTACGGGAGGCAGCAG-30. Libraries were sequenced on an Illumina MiSeq platform according to the standard protocols. Analyses were performed with the Quantitative Insights Into Microbial Ecology 2 (QIIME2-2018.4; https://qiime2.org) software suite [28], using quality filtering and analysis parameters as described in the Supplemental Experimental Procedures.

Statistical analysis

For all analyses, the individual mouse was considered the experimental unit within the studies. Experimental design was planned using the Experimental Design Assistant [29]. A multi-replica design was used, where each replica was run completely independently. Within each replica there were concurrent controls of infected and non-infected animals. The number of animals for each genotype within a replica varies as it was constrained by the outcome of breeding.

The effect of genotype on worm burden within infected mice was assessed across multiple replicas using an Integrative Data Analysis (IDA) [30] treating each replica as a fixed effect utilising the generalised least square regression function within the nlme version 3.1 package of R (version 3.3.1). A likelihood ratio test was used to test for the role of genotype by comparing a test model (Eq 1) against a null model (Eq 2). As genotype was found to be highly significant in explaining variation, a F ratio test for Eq 1 was used to explore the role of genotype as a main effect and whether it interacted with sex. The effect of genotype was not found to interact with sex ($p>0.05$).

$$\text{Worm burden} = \beta_0 + \beta_1\text{Genotype} + \beta_2\text{Replica} + \beta_3\text{Sex} + \beta_4\text{Sex} * \text{Genotype} \quad \text{[Eq 1]}$$

$$\text{Worm burden} = \beta_0 + \beta_1\text{Replica} + \beta_2\text{Sex} \quad \text{[Eq 2]}$$

The effect of gene knockout on worm burden was assessed for each sex separately using a

Mann Whitney U test from the Prism 7.0 software (GraphPad). This analysis pools data across replicas as the IDA analysis found that this was not a significant source of variation. A non-parametric test was used as the data is bound and has some non-normal distribution characteristics. Similarly, cytokine levels between infected WT and mutant mice and plasma chemistry parameters between infected isotype and IL-10Rα -treated *Rag1*^{tm1Mom} mice were evaluated using a Mann Whitney U test from the Prism 7.0 software (GraphPad).

The survival data, pooled across replicas, was tested for a significant effect of gene knockout for each sex independently using Log-rank Mantel-Cox tests from the Prism 7.0 software (GraphPad).

To evaluate the effect of the degree of colonization by pathobionts on the survival of infected IL-10 signalling-deficient mice, the mice were classified based on the histological assessment of the liver and survival time (time after infection that mice succumbed), into two groups: severe (presence of granulomas necrosis and foamy macrophages in the liver, weight loss and poor survival) and mild (minor liver infiltration, no weight loss and extended survival). Next, the degree of colonization by *Enterococcus*, *Enterobacteriaceae* and *Escherichia-Shigella* (combined percentage of abundance of these three groups from total microbiota) among both groups was compared using a Mann Whitney U test from the Prism 7.0 software (GraphPad). In addition, a correlation analysis of the degree of colonization of the pathobionts and the plasma levels of the liver enzyme aspartate aminotransferase was performed using a two-tailed Spearman correlation test.

A similar IDA analysis was used to study the effect of genotype on infection, for each plasma chemistry variable across multiple replicas. In this IDA, a likelihood ratio test was used to test for an interaction between genotype and infection by comparing a test model (Eq 3) against a null model (Eq 4). This regression model was fitted to separate the various sources of variation allowing the impact of genotype in the presence of infection to be estimated.

$$Y = \beta_0 + \beta_1 \text{Replica} + \beta_2 \text{Genotype} + \beta_3 \text{Sex} + \beta_4 \text{Sex} * \text{Genotype} + \beta_5 \text{Infection} : \text{Genotype} \quad \text{[Eq 3]}$$

$$Y = \beta_0 + \beta_1 \text{Replica} + \beta_2 \text{Genotype} + \beta_3 \text{Sex} + \beta_4 \text{Sex} * \text{Genotype} + \beta_5 \text{Infection} \quad \text{[Eq 4]}$$

P-values were adjusted for multiple testing using the Benjamini and Hochberg method [31] with a false discovery rate of 5%. Percentage change was calculated to allow comparison of the effect across variables by taking the estimated coefficient from the regression analysis and dividing it by the average signal seen for that variable. The model estimates without normalisation are presented in S4 Table.

The effect of genotype and infection on caecum score and goblet cells per crypt was assessed across the multiple replicas using an IDA as described for the plasma chemistry variables.

For all IDAs, the model fit was assessed by visual exploration of the residuals with quantile-quantile and residual-predicted plots for each genotype group.

Results

The host response to *T. muris* infection does not require IL-22 and IL-28 signalling

To dissect the role of the members of the IL-10 family of receptors during whipworm infection, mouse lines with knockout mutations for the following loci were challenged with *T. muris*: *Il10*, *Il10ra*, *Il10rb*, *Il22*, *Il22ra* and *Il28ra* (*S1 Fig*). The influence of these mutations on anti-parasite immunity and worm expulsion was evaluated. Like WT mice, a high dose infection with *T. muris* did not result in chronic infection of IL-22, IL-22Rα and IL-28Rα mutant

mice; after 32 days of infection, the mice had expelled all worms and had high levels of parasite specific IgG1 in their sera that indicated the development of a type-2 response *(S2A, S2B* and *S2C Fig)*. Moreover, worm expulsion occurred before day 21 post infection (p.i.), accompanied by production of *T. muris* specific IgG1 (*S3A, S3B* and *S3C Fig)*. These results are contrary to previous reports describing delayed worm expulsion in IL-22 mutant mice at day 21p.i. [22].

Using low dose infections, at day 35 p.i., there were also no differences between WT and IL-22, IL-22Rα and IL-28Rα mutant mice in the establishment of a chronic infection that is characterized by high levels of parasite specific IgG2a/c in serum (*S4A, S4B* and *S4C Fig)*. These findings indicated that IL-22 and IL-28 signalling are dispensable for the host to mount a response to *T. muris* infection. When taken together with previous data, these results suggest that the IL-10 receptor is the only member from this family of receptors responsible for the control of host resistance and survival to whipworm infection.

IL-10 signalling is essential to control caecal pathology, worm expulsion and mouse survival during *T. muris* infections

We then examined the contribution of IL-10 signalling to the responses to *T. muris* infection. IL-10, IL-10Rα and IL-10Rβ mutant mice were infected with a high dose of eggs and survival, tissue histopathology and worm burdens throughout infection up to day 28 p.i. were evaluated. We used WT littermate controls that were co-housed with the mutant mice throughout the experiments. Moreover, we included uninfected WT and mutant mice as additional controls in the cages. IL-10, IL-10Rα and IL-10Rβ mutant mice did not develop spontaneous colitis in our mouse facility.

As previously reported [8], female and male IL-10 mutant mice succumbed to whipworm infection between day 19 and 24 p.i., showing a dramatic weight loss and high numbers of worms in the caecum when compared with WT mice *(Fig 1A)*. Similarly, female and male IL-10Rα mutant mice displayed weight loss and all required euthanasia by day 28p.i. concomitant with high worm burdens in the caecum *(Fig 1B)*. Although the defects in the expulsion of worms in IL-10Rα mutant mice have been described [21], this is the first report of reduced survival of these mice upon whipworm infection. Likewise, high numbers of worms were present in the caecum of IL-10Rβ mutant mice and survival was reduced by 60% and 75% in females and males, respectively *(Fig 1C)*. Defective worm expulsion and survival in *T. muris*-infected IL-10, IL-10Rα and IL-10Rβ mutant mice correlated with increased inflammation in the caecum *(Fig 2)*. Specifically, while infected WT mice presented mild inflammation *(Fig 2A and 2B)* and goblet cell hyperplasia *(Figs 2C and S5)*, a characteristic response to *T. muris*, infected IL-10 signalling-deficient mice displayed submucosal oedema, large inflammatory infiltrates in the mucosa with villous hyperplasia, distortion of the epithelial architecture *(Fig 2A and 2B)* and loss of goblet cells *(Figs 2C and S5)*. Together, these results indicate that during *T. muris* infections, IL-10 signalling is crucial for controlling worm expulsion and caecal mucosal and submucosal inflammation leading to unsustainable pathology.

Defects in IL-10 signalling result in liver immunopathology and systemic inflammatory responses during whipworm infection

Reduced survival of whipworm-infected IL-10 signalling-deficient mice correlated with liver pathology, while we did not observe pathology in other systemic organs such as the spleen. Specifically, upon culling and dissection of *T. muris*-infected IL-10, IL-10Rα and IL-10Rβ mutant mice, we observed granulomatous lesions in their livers including necrotic areas and lymphocytic and phagocytic infiltrates *(Fig 3)*. Moreover, 50, 25 and 12.5% of *T. muris*-infected IL-10, IL-10Rα and IL-10Rβ mutant mice, respectively, showed extensive numbers of foamy

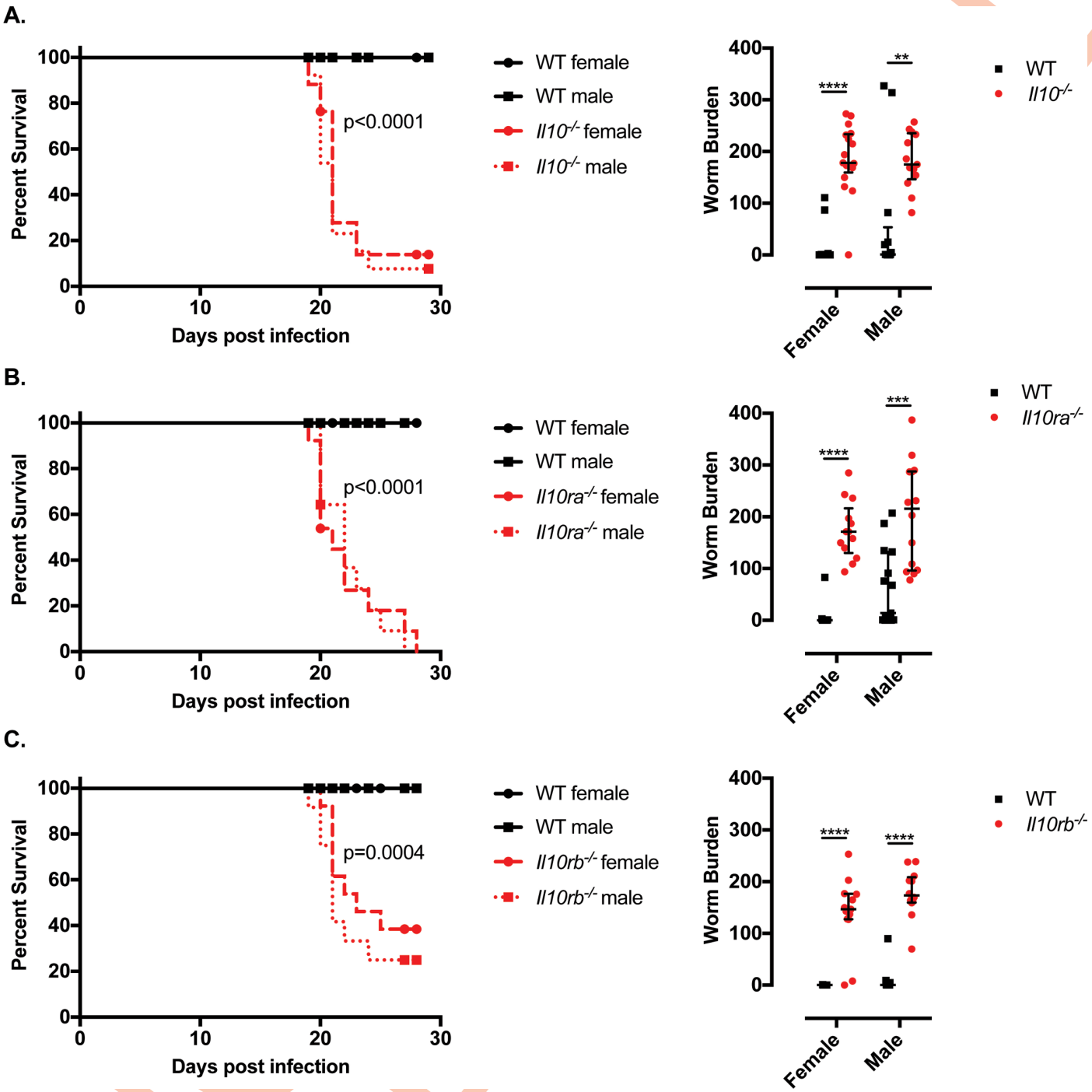

Fig 1. Defective IL-10 signalling results in failed worm expulsion and reduced survival upon *T. muris* infection. Survival curves and worm burdens of *T. muris*-infected (high dose, 400 eggs), six-wk-old female and male littermate WT and (A) *Il10*$^{-/-}$, (B) *Il10ra*$^{-/-}$, (C) *Il10rb*$^{-/-}$ mice. For worm burden, median and interquartile range are shown and the effect of genotype from the IDA analysis is highly significant (A) p = 5.15e-11, (B) p = 2.92e-11 and (C) p = 4.44e-16. (A) Data from five independent replicas. WT female n = 18. WT male n = 13. *Il10*$^{-/-}$ female n = 17. *Il10*$^{-/-}$ male n = 13. Log-rank Mantel-Cox test for survival curves. Mann Whitney U Test for worm burdens, ****p<0.001, **p = 0.002. (B) Data from five independent replicas. WT female n = 16. WT male n = 15. *Il10ra*$^{-/-}$ female n = 13. *Il10ra*$^{-/-}$ male n = 14. Log-rank Mantel-Cox test for survival curves. Mann Whitney U Test for worm burdens, ****p<0.001, ***p = 0.0002. (C) Data from four independent replicas. WT female n = 11. WT male n = 12. *Il10rb*$^{-/-}$ female n = 13. *Il10rb*$^{-/-}$ male n = 12. Log-rank Mantel-Cox test for survival curves. Mann Whitney U Test for worm burdens, ****p<0.001.

https://doi.org/10.1371/journal.ppat.1007265.g001

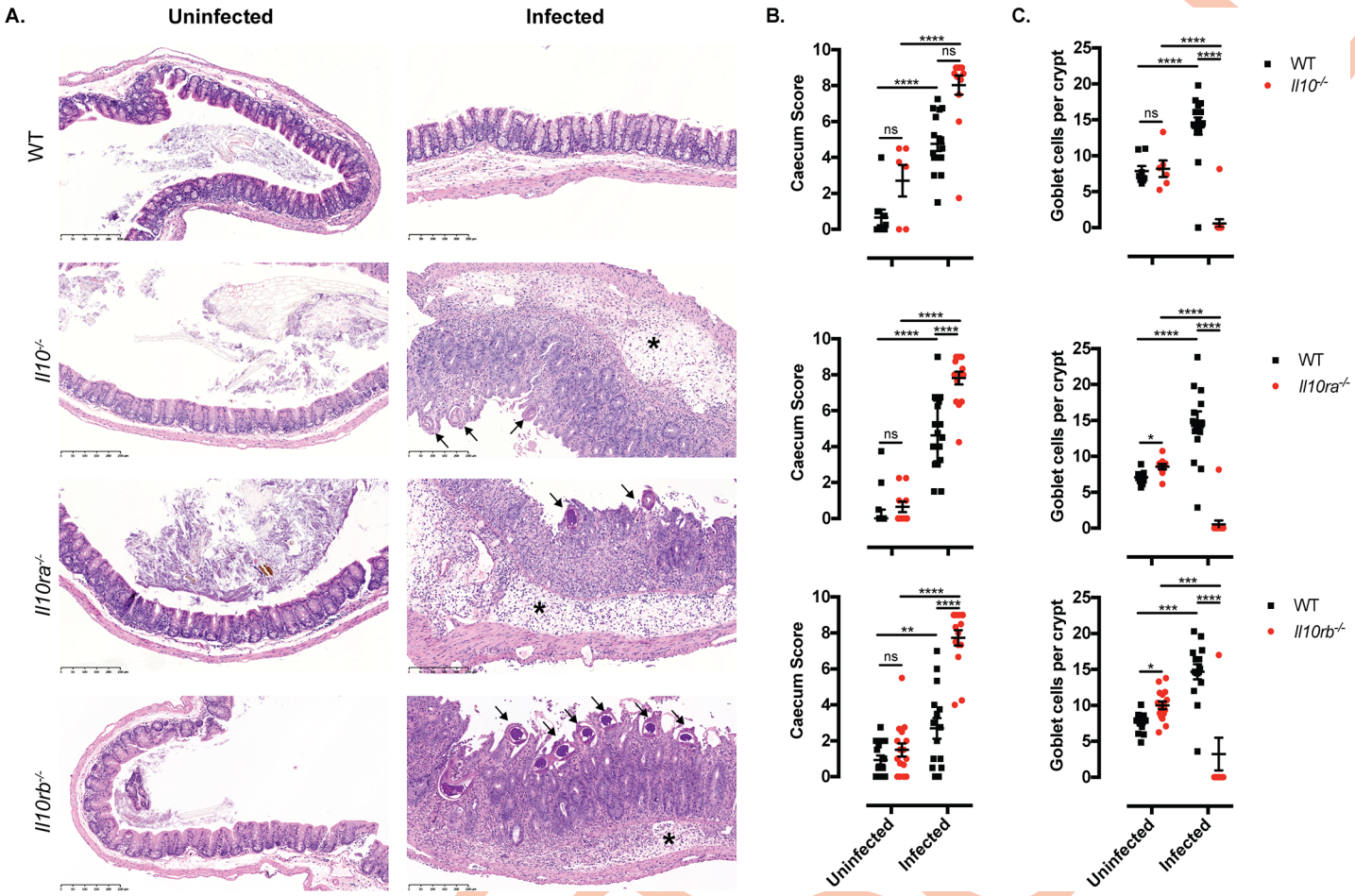

Fig 2. IL-10 signalling controls caecal immunopathology maintaining epithelial architecture during *T. muris* infection. Caecal histopathology of uninfected and *T. muris*-infected (high dose, 400 eggs) WT, *Il10*$^{-/-}$, *Il10ra*$^{-/-}$ and *Il10rb*$^{-/-}$ mice upon culling. (A) Representative images from sections stained with H&E. Uninfected WT and mutant mice show no signs of inflammation. Upon infection, WT mice present goblet cell hyperplasia and IL-10 signalling-deficient mice show submucosal oedema (asterisks) and large inflammatory infiltrates in the mucosa with villous hyperplasia and distortion of the epithelial architecture. *T. muris* worms are infecting the mucosa (arrows) of IL-10 signalling-deficient mice. Scale bar, 250μm. (B) Caecum inflammation scores and (C) goblet cells numbers per crypt were blindly calculated for each section. Data from two independent replicas (n = 5–18 each group). Mean and standard error of the mean (SEM) are shown. IDA analysis, $^{****}p<0.0001$, $^{***}p<0.0005$, $^{**}p<0.005$, $^{*}p<0.05$.

https://doi.org/10.1371/journal.ppat.1007265.g002

(lipid-loaded) macrophages in their livers (*S6 Fig*). Because survival upon whipworm infection is similarly reduced among IL-10, IL-10Rα and IL-10Rβ mutant mice but IL-10Rα is the only subunit that is exclusively used for IL-10 signalling, we focused subsequent experiments on IL-10Rα-deficient mice.

Liver disease was reflected in changes to plasma chemistry markers of liver damage. Compared to WT mice, *T. muris*-infected mice with defects in IL-10 signalling presented significantly dysregulated plasma levels of liver enzymes (decreased concentrations of alkaline phosphatase and increased concentrations of aspartate and alanine aminotransferase), accompanied by reduced concentrations of glucose, fructosamine, albumin and thyroxine (*Figs 4A and S7*). Upon whipworm infection, we also observed augmented levels of ferritin and transferrin, which are indicators of systemic infection, in IL-10 signalling-deficient, but not in WT mice (*Figs 4A and S7*). We found no or minimal differences in plasma chemistry between uninfected WT and mutant mice (S1, S2 and S3 Tables). The changes in plasma chemistry

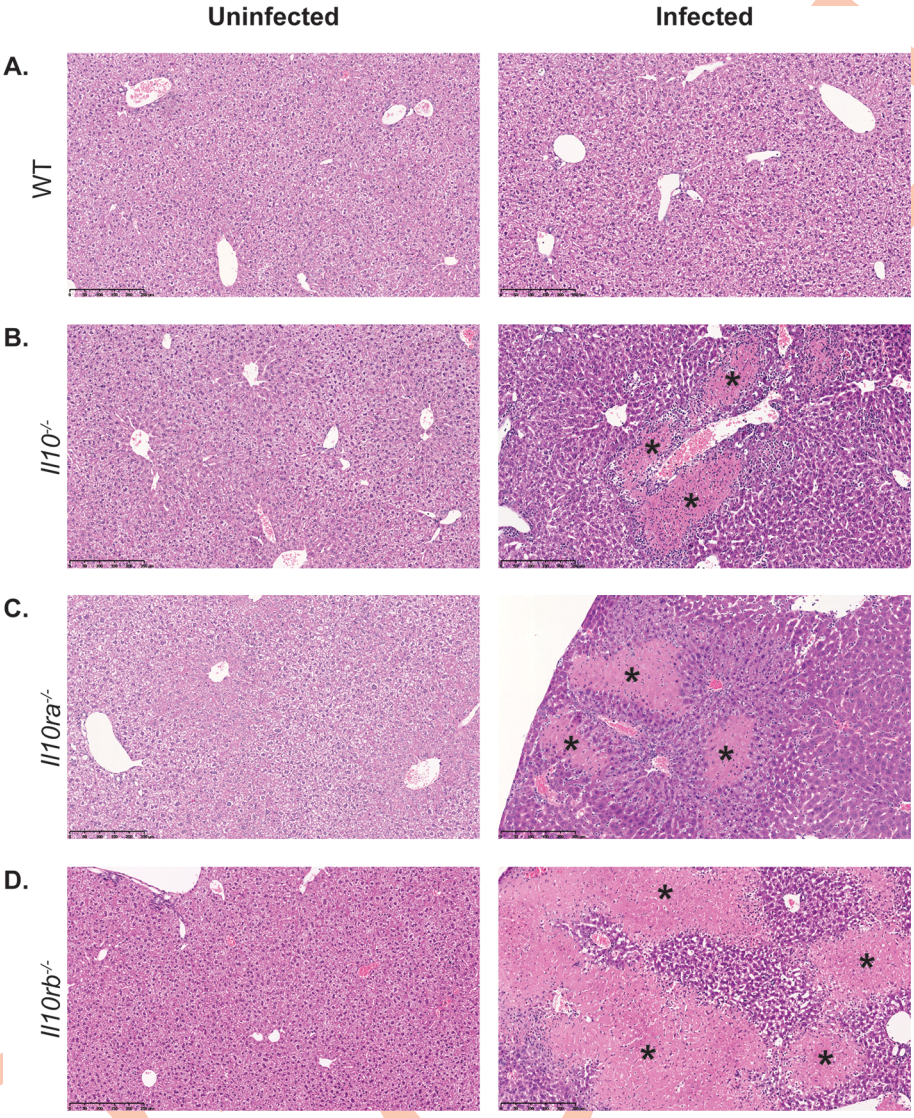

Fig 3. IL-10 signalling prevents liver immunopathology upon whipworm infection. Liver histopathology of uninfected and *T. muris*-infected (high dose, 400 eggs) (A) WT, (B) *Il10*$^{-/-}$, (C) *Il10ra*$^{-/-}$ and (D) *Il10rb*$^{-/-}$ mice upon culling. Representative images from sections stained with H&E. Uninfected WT and mutant mice show no lesions. Upon infection, some IL-10 signalling-deficient mice show necrotic granulomatous lesions with inflammatory infiltrate (asterisks). Scale bar, 250μm. Results are from two independent replicas (n = 5–18 each).

https://doi.org/10.1371/journal.ppat.1007265.g003

parameters between infected WT and mutant mice were accompanied by increased circulating concentrations of the inflammatory cytokines IL-6 and TNF-α (*Figs 4B* and *4C and S8*).

Liver pathology appears to be caused by dissemination of gut bacteria or their products to the liver, upon breakdown of the caecal epithelial barrier due to whipworm infection and IL-10 signalling defects.

Lack of IL-10 signalling leads to caecal dysbiosis during *T. muris* infection

Outgrowth of opportunistic bacteria contributes to the mortality of IL-10 mutant mice during whipworm infection [8, 20]. Furthermore, intestinal inflammation can promote microbial dysbiosis and impair resistance to colonization by opportunistic pathogens [32, 33]. We hypothesised that infection of IL-10 signalling-deficient mice with whipworms caused caecal dysbiosis

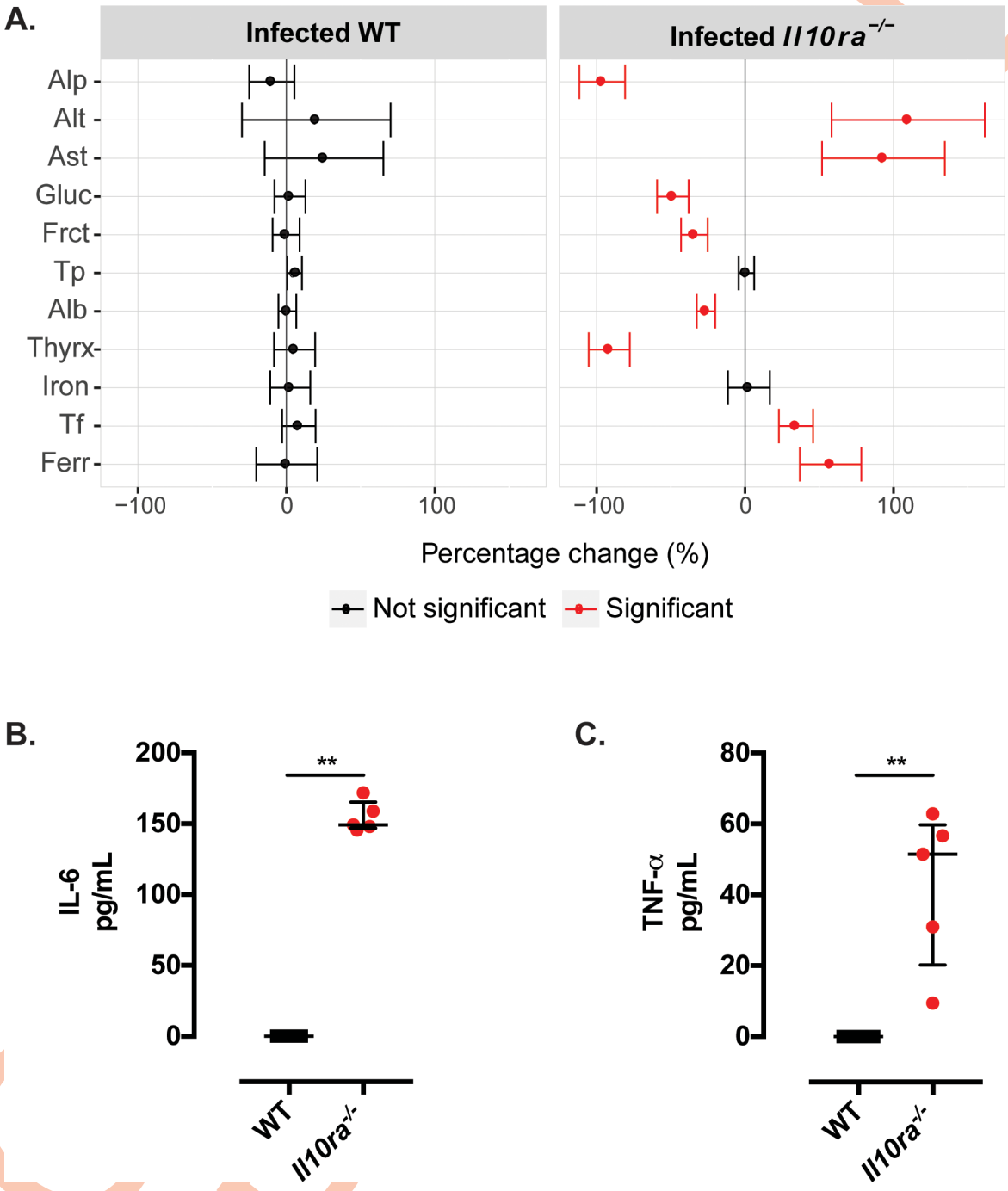

Fig 4. Whipworm infection of defective IL-10 signalling mice results in liver disease and systemic inflammatory responses. Percentage change of plasma chemistry parameters (A) and IL-6 (B) and TNF-α (C) concentrations in plasma of *T. muris*-infected (high dose, 400 eggs), six-wk-old female and male littermate WT and *Il10ra*$^{-/-}$ mice culled upon deterioration of the mice condition. (A) The infection status effect on each genotype for plasma chemistry parameters associated with liver disease was estimated across three independent replicas. The estimate has been visualised as a percentage normalised value (signal/average signal for that parameter) along with the 95% confidence interval to allow comparison across variables. Highlighted in red, are parameters where the genotype by infection is statistically significant in explaining variation after adjustment for multiple testing (5% FDR) and are significant in the final model estimate ($p<0.05$). WT n = 25. *Il10ra*$^{-/-}$ n = 22. Alkaline phosphatase (Alp), alanine aminotransferase (Alt), aspartate aminotransferase (Ast), glucose (Gluc), fructosamine (Fruct), total protein (Tp), albumin (Alb), thyroxine (Thyrx), transferrin (Tf) and ferritin (Ferr). (B and C) Median and interquartile range are shown. WT n = 5. *Il10ra*$^{-/-}$ n = 5. Mann Whitney U Test, $^{**}p = 0.002$. Results are from two independent replicas.

https://doi.org/10.1371/journal.ppat.1007265.g004

and the overgrowth of opportunistic bacteria from the microbiota. Thus, we analysed the microbiota composition of uninfected and *T. muris*-infected WT and IL-10, IL-10Rα and IL-10Rβ mutant mice using high-throughput 16S rRNA sequencing. No significant differences in overall gut microbial profiles and alpha/beta diversity were detected between uninfected IL-10 signalling-deficient and WT mice *(S9, S10* and *S11 Figs)*, thus indicating that IL-10 signalling did not impact caecal microbial community structure, an observation that is consistent with the lack of spontaneous inflammation in these mice in our mouse facility. Similarly, whipworm infection of WT mice did not lead to changes in overall microbial community structure and alpha/beta diversity, as shown by the lack of significant differences between the gut microbial profiles of infected and uninfected WT mice *(S9, S10* and *S11 Figs)*. Conversely, whipworm infection of IL-10Rα mutant mice resulted in a caecal microbial profile distinct from that of infected WT mice ($p = 0.001$, CCA, *Fig 5A)*, but also of uninfected WT and mutant mice, as shown by both PCoA and CCA (*S10A Fig)*. The observed changes in the caecal microbial community structure were associated with a significant increase in microbial beta diversity (i.e. differences in species composition between groups; $p = 0.001$, ANOSIM; *Fig 5B)* and a decrease in alpha diversity (i.e. species diversity within a group) (measured through Shannon diversity, $p = 0.01$, ANOVA; *Fig 5C*) in *T. muris*-infected IL-10Rα mutant mice when compared to WT and uninfected mice (*S10B and S10C Fig*). In particular, the observed decrease in alpha diversity of the caecal microbiota in *T. muris*-infected IL-10Rα mutant mice was associated with significant reductions of both microbial richness (i.e. the number of species composing the microbial community; $p < 0.001$, ANOVA; *Figs 5C and S10C*) and evenness (i.e. the relative abundance of each microbial species in the community; $p < 0.001$, ANOVA; *Figs 5C and S10C*). Network analysis identified a positive correlation between the presence and relative abundance of several opportunistic pathogens (i.e. *Enterobacteriaceae*, *Escherichia/Shigella*, *Enterococcus*, and *Clostridium difficile*), as well as lactic acid-producing bacteria (i.e. *Lactobacillus*), and the microbial profiles of *T. muris*-infected IL-10Rα mutant mice (*Fig 5D*). Moreover, analysis of differential abundance of individual bacterial taxa via Linear Discriminant Analysis Effect Size (LEfSe) revealed that *Enterobacteriaceae*, *Enterococcaceae* and *Lactobacillaceae* were significantly more abundant in infected mutant mice, than in any of the other mouse groups (LDA Score (log10) of 4.78, 4.77, and 4.44 respectively; *Figs 5E* and *S10E*). The increase in abundance of these groups in the *T. muris*-infected IL-10Rα mutant mice was also observed when comparing the relative OTU abundances (*Fig 5F*).

Similarly, *T. muris*-infected IL-10 and IL-10Rβ mutant mice presented a clear and consistent overgrowth of *Enterobacteriaceae*, *Escherichia/Shigella* and *Enterococcus (S9 and S11 Figs)*. The degree of colonization by these pathobionts correlated with the reduced survival (time after infection that mice succumbed) and extent of liver disease observed *(S12 Fig)*. Co-housing of the uninfected and *T. muris*-infected WT and mutant mice did not result in microbiota transfer by coprophagia as the dysbiosis and presence of pathobionts in the infected mutant mice was not observed in any other groups *(S9, S10 and S11 Figs)*.

Altogether these results indicate that absence of IL-10 signalling during whipworm infection causes intestinal dysbiosis due to the overgrowth of facultative anaerobes, members of the microbiota that have been previously described as opportunistic pathogens [34–36]. Moreover, the presence of the parasite is critical to the development of the observed dysbiotic state.

IL-10 signalling maintains the caecal epithelial barrier preventing microbial translocation to the liver during *T. muris* infection

We hypothesized that the opportunistic pathogens (or their products) present in the dysbiotic microbiota of the whipworm-infected IL-10 signalling-deficient mice were disseminating to

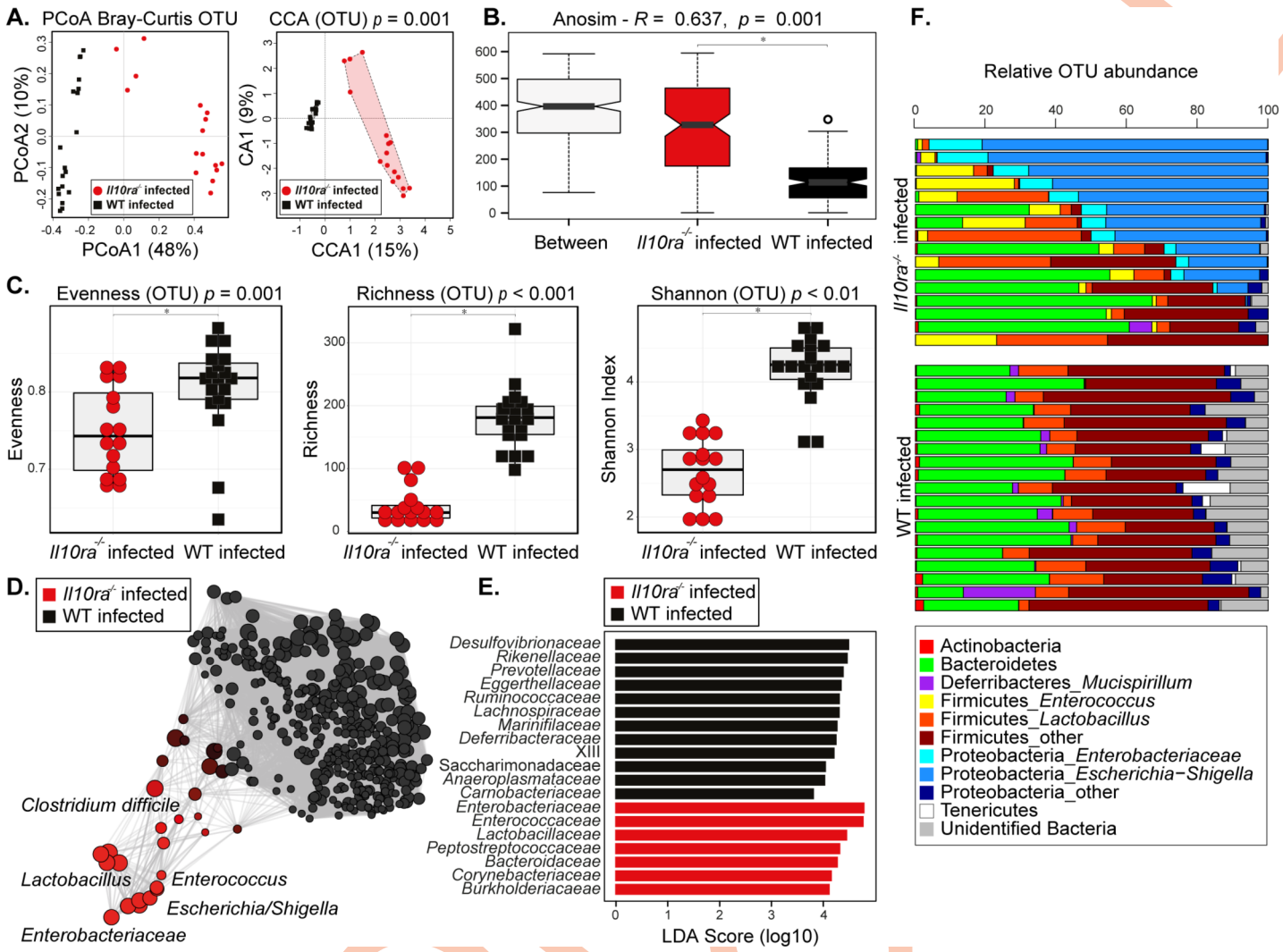

Fig 5. Caecal dysbiosis upon whipworm infection and defective IL-10 signalling is associated with expanded populations of pathobionts. Caecal microbial community structure at the operational taxonomic unit (OTU) level of co-housed *T. muris*-infected (high dose, 400 eggs) six-wk-old female and male littermate WT and *Il10ra*$^{-/-}$ mice at day of culling. (A) Principal Coordinates Analysis (PCoA) and Canonical Correspondence Analysis (CCA p = 0.001), the numbers in brackets indicate the percentage variance explained by that component. (B) beta-diversity index (ANOSIM R = 0.637 and p = 0.001), (C) alpha-diversity indexes (Shannon diversity, richness and evenness; ANOVA p = 0.01, p<0.001, p<0.001, respectively), (D) network analysis, (E) Linear Discriminant Analysis Effect Size (LEfSe) analysis and (F) bar plots representing proportional abundance of individual OTUs in caecal microbial community structures. Data from two independent replicas. WT n = 19. *Il10ra*$^{-/-}$ n = 16.

https://doi.org/10.1371/journal.ppat.1007265.g005

the liver, thus causing lethal disease. To test this hypothesis, we examined whether a breakage of the epithelial barrier allowed bacteria from the *Escherichia* and the *Enterococcus* genera to translocate intracellularly through the caecal epithelia. Immunofluorescence labelling for the tight junction protein ZO-1, showed that in contrast to WT mice that have expelled the worms, and in which tight junctions are intact *(Fig 6A)*, whipworm-infected IL-10Rα-deficient mice lacked tight junctions in regions of the caecal epithelia replaced with high inflammatory infiltrate (Fig 6B and 6D). Transmission electron microscopy of those regions clearly showed a neutrophilic infiltrate and the denuded epithelium *(Fig 6E and 6F)*. Tight junctions of cells in close proximity to the worm are also lost (Fig 6C). Moreover, using transmission electron microscopy, we observed the presence of intracellular cocci and bacilli in the caecal epithelia

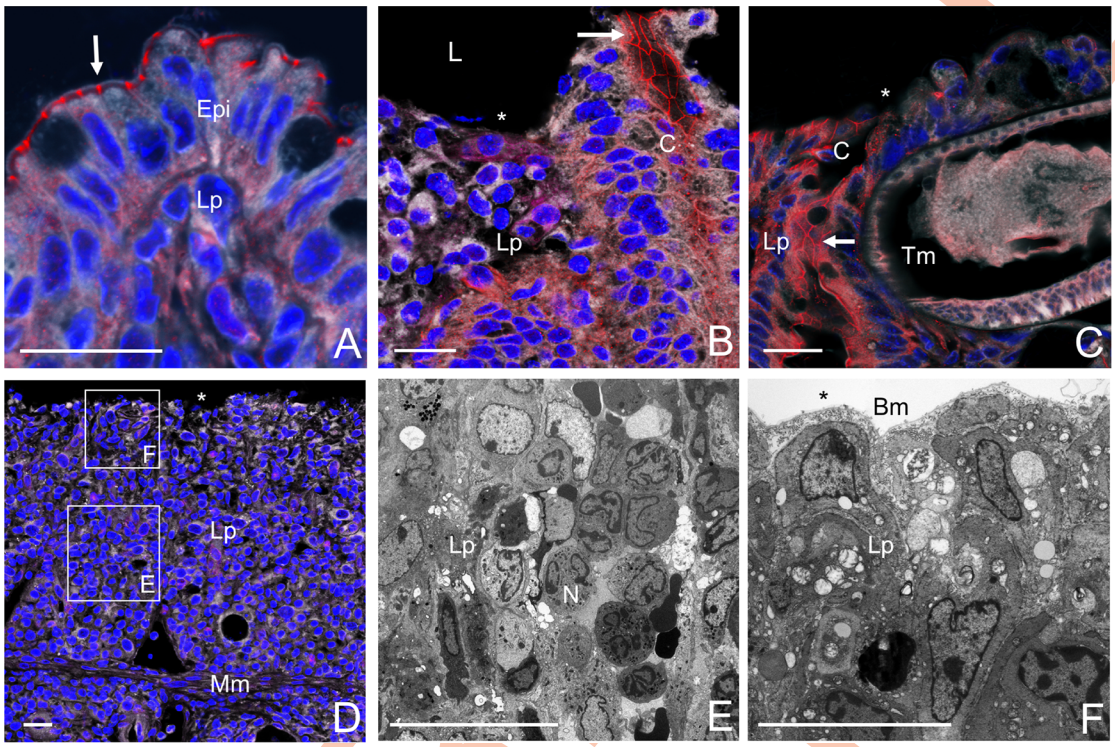

Fig 6. Defective IL-10Rα signalling during *T. muris* infection results in caecal epithelial barrier breakage. (A) Representative immunofluorescence images of intact tight junctions (ZO-1 positive cells) in epithelium of whipworm-infected WT mice. (B-F) Epithelial barrier breakage in whipworm-infected IL-10Ra mutant mice. Representative immunofluorescence images of denuded epithelium with lack of tight junctions in areas with inflammatory infiltrate (B, D) and cells surrounding whipworms (C). Representative electron micrographs of regions E and F in the inflammatory infiltrate of panel D (D-E). Red, tight junction protein ZO-1; grey, membranes; and blue, cell nuclei. Tight junctions (arrows), denuded epithelium (asterisks), Lp = lamina propria, Mm = lamina muscular mucosa, L = lumen, C = crypt, N = neutrophil, Bm = basement membrane, Epi = epithelium, Tmt = *T. muris* tegument. Scale bar, 20μm. Results are from two independent replicas (n = 3–4 each).

https://doi.org/10.1371/journal.ppat.1007265.g006

of whipworm-infected IL-10 signalling-deficient, but not WT mice *(Fig 7A)*. Immunofluorescence staining with antibodies against *Escherichia* spp. and *Enterococcus* spp. further indicated the intracellular translocation of these opportunistic pathogens through the enterocytes of the caecum of whipworm-infected IL-10 signalling-deficient mice *(Fig 7B and 7C)*. These observations indicate that both *Escherichia* spp. and *Enterococcus* spp. invade the caecal epithelium of IL-10 signalling-deficient mice upon whipworm infection. Furthermore, they suggest that translocation of these opportunistic pathogens or their products to the liver are the potential cause of lethal liver disease observed in these mice.

Livers of *T. muris*-infected WT and IL-10 signalling-deficient mice were cultured under aerobic and anaerobic conditions to identify bacterial isolates using 16S rRNA sequencing. We found *E. coli*, *E. faecalis and E. gallinarum* in the livers of some whipworm-infected IL-10 signalling-deficient but not in WT mice (S5, S6 and S7 Tables). Moreover, using 16S rRNA PCR and sequencing, we found *Escherichia/Shigella* and *Enterococcus* were more abundant in whipworm infected IL-10Rα–deficient mice than in uninfected WT and IL-10Rα–deficient mice and for *Enterococcus* this was also significant when comparing with infected WT mice (*Fig 8A–8C*). Although systematically examining entire livers was not feasible, we did observe bacteria staining with the *Escherichia* spp. and *Enterococcus* spp. antibodies in the sections from livers of some whipworm-infected IL-10 signalling-deficient mice but not in whipworm-infected WT mice *(Fig 8D and 8E)*.

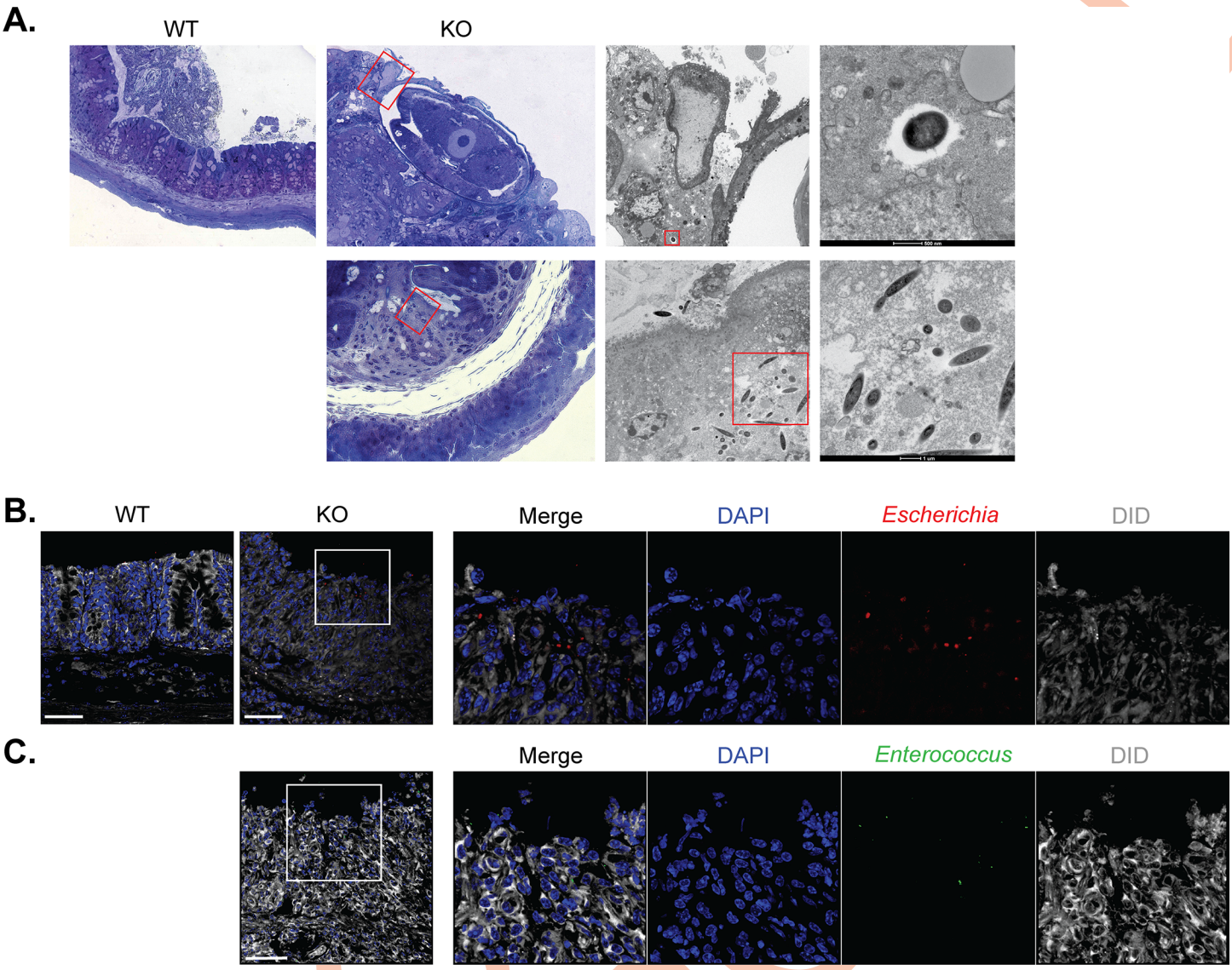

Fig 7. IL-10 signalling during *T. muris* infection maintains intestinal barrier limiting *Enterococcus* and *Escherichia* bacterial translocation through the caecal epithelium. (A) Representative transmission electron micrographs of *T. muris*-infected WT and IL-10 signalling-deficient mice (*Il-10*, *Il10ra*$^{-/-}$ and *Il10rb*$^{-/-}$) caecal tissues, showing translocation of cocci and rod-like bacteria. (B) Representative immunofluorescence of *Escherichia* spp. in the caecum of *T. muris*-infected WT and IL-10 signalling-deficient mice (*Il-10*, *Il10ra*$^{-/-}$ and *Il10rb*$^{-/-}$). DiD stains membranes and DAPI stains cell nuclei. Scale bar, 50 μm. (C) Representative immunofluorescence of *Enterococcus* spp. in the caecum of *T. muris*-infected WT and IL-10 signalling-deficient mice (*Il-10*, *Il10ra*$^{-/-}$ and *Il10rb*$^{-/-}$). DiD stains membranes and DAPI stains cell nuclei. Scale bar, 50 μm. Results are from two independent replicas (n = 3–4 each).

https://doi.org/10.1371/journal.ppat.1007265.g007

In summary, our findings indicate that IL10 signalling, via the IL-10Rα and IL-10Rβ, promotes resistance to colonization by opportunistic pathogens and controls immunopathology preventing microbial translocation and lethal disease upon whipworm infection.

Control of immunopathology, worm expulsion and survival require signalling through IL-10Rα and IL-10Rβ in haematopoietic cells

Conditional knockout mice lacking IL-10Rα on T cells and monocytes/macrophages/neutrophils did not recapitulate the phenotype of the complete mutant, thus suggesting that these cell types alone are not the main responders to IL-10 during whipworm infection [21]. This

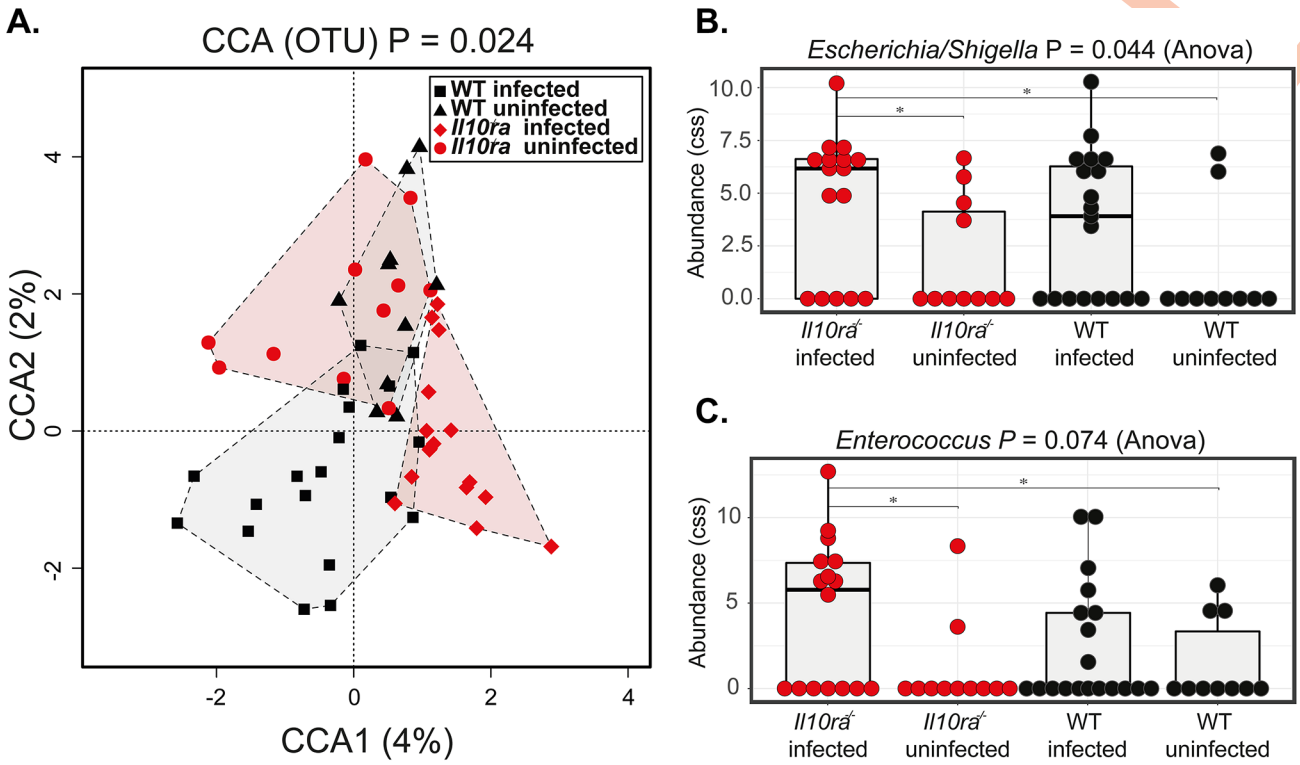
A.
CCA (OTU) P = 0.024
WT infected
WT uninfected
Il10ra infected
Il10ra uninfected
CCA2 (2%)
CCA1 (4%)
B.
Escherichia/Shigella P = 0.044 (Anova)
Abundance (css)
Il10ra-/- infected
Il10ra-/- uninfected
WT infected
WT uninfected
C.
Enterococcus P = 0.074 (Anova)
Abundance (css)
Il10ra-/- infected
Il10ra-/- uninfected
WT infected
WT uninfected

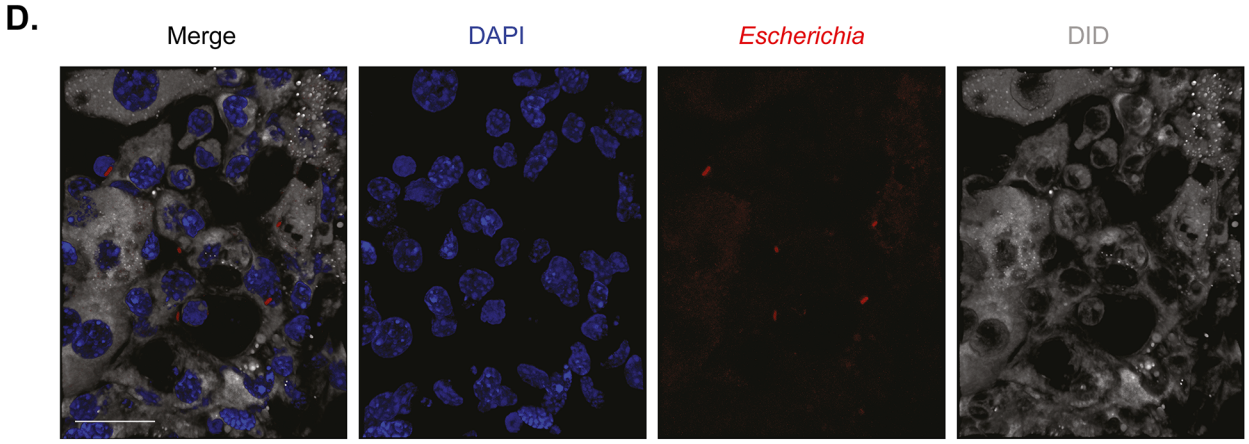
D.
Merge
DAPI
Escherichia
DID

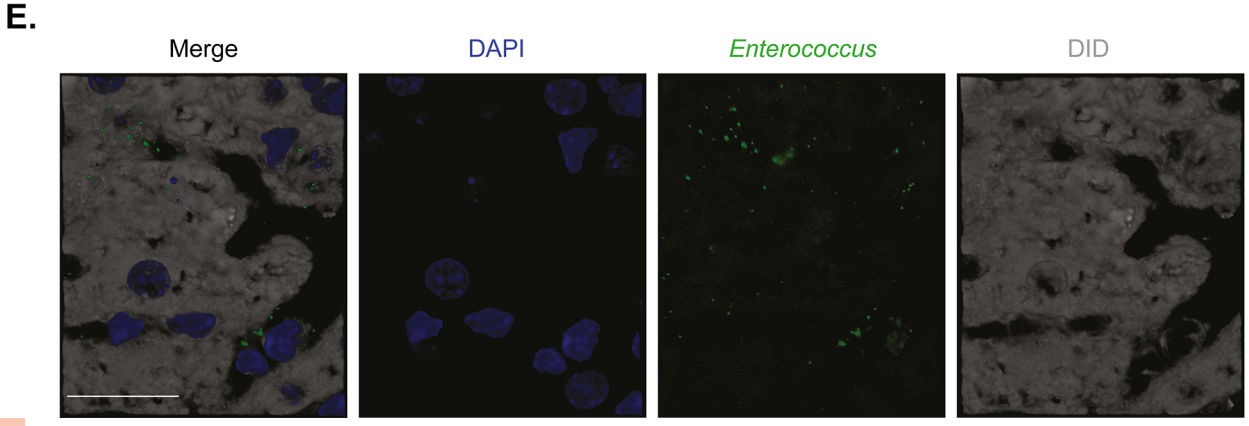
E.
Merge
DAPI
Enterococcus
DID

Fig 8. IL-10 signalling during *T. muris* infection limits *Enterococcus* and *Escherichia* bacterial translocation to the liver, protecting from lethal disease. Liver microbial community structure at the operational taxonomic unit (OTU) level of uninfected and *T. muris*-infected (high dose, 400 eggs) six-wk-old female and male littermate WT and *Il10ra*$^{-/-}$ mice at day of culling. (A) Canonical Correspondence Analysis (CCA p = 0.024), the numbers in brackets indicate the percentage variance explained by that component. Bar plots representing normalised proportional abundance of (B) *Escherichia/Shigella* and (C) *Enterococcus* OTUs in the liver (Kruskal-Wallis Test p = 0.01, p = 0.011, respectively. Mann Whitney Test for intergroup comparisons). Data from two independent replicas. WT uninfected n = 10. WT infected n = 19. *Il10ra*$^{-/-}$ uninfected n = 11. *Il10ra*$^{-/-}$ infected n = 16. (D) Representative immunofluorescence of *Escherichia* spp. in the liver of *T. muris*-infected IL-10 signalling-deficient mice (*Il-10*, *Il10ra*$^{-/-}$ and *Il10rb*$^{-/-}$). DiD stains membranes and DAPI stains cell nuclei. Scale bar, 20 μm. (E) Representative immunofluorescence of *Enterococcus* spp. in the liver of *T. muris*- IL-10 signalling-deficient mice (*Il-10*, *Il10ra*$^{-/-}$ and *Il10rb*$^{-/-}$). DiD stains membranes and DAPI stains cell nuclei. Scale bar, 20 μm. For D and E, results are from two independent replicas (n = 3–4 each).

https://doi.org/10.1371/journal.ppat.1007265.g008

indicates that expression of IL-10Rα on other immune cells or IECs or in a combination of effector cells may be responsible for the IL-10 effects on worm expulsion and inflammatory control. To identify whether the main target cells of IL-10 were of haematopoietic or non-haematopoietic (epithelial) origin, we generated bone marrow chimeric mice by transferring either WT or IL-10Rα and IL-10Rβ–deficient bone marrow into lethally irradiated WT or IL-10Rα and IL-10Rβ–deficient mice and infected them with a high dose of *T. muris*. We observed decreased survival around day 20p.i. of 100% of irradiated WT mice reconstituted with bone marrow of IL-10Rα and IL-10Rβ mutant donors *(Figs 9A and S13A)*, which was accompanied by caecal and liver pathology *(Figs 9B and S13B)*. By contrast, WT mice receiving bone marrow cells from WT donors did not show any morbidity signs or caecal inflammation, even when worm expulsion was not always observed *(Figs 9A and S13A)*. Conversely, reconstitution of irradiated IL-10Rα and IL-10Rβ mutant mice with WT donor bone marrow protected them from the unsustainable pathology caused by whipworm infection *(Figs 9C and 9D and S13C and S13D)*. These results suggest that the main target cells responding to IL-10 are of haematopoietic origin.

To support these findings and overcome the limitations of bone marrow chimera mice that include incomplete immune system reconstitution and microbiota dysregulation, we generated conditional mutant mice for the IL-10Rα on IECs (*Il10ra*$^{fl/fl}$ *Vil*$^{cre/+}$) and infected them with a high dose of *T. muris*. Similar to WT controls (*Il10ra*$^{+/+}$ *Vil*$^{cre/+}$ and *Il10ra*$^{fl/fl}$ *Vil*$^{+/+}$), *Il10ra*$^{fl/fl}$ *Vil*$^{cre/+}$ mice expelled the worms as early as day 20 p.i. and developed a type 2 response indicated by the presence of specific parasite IgG1 antibodies in the serum *(S14 Fig)*.

To further investigate which cells of haematopoietic origin are mediating the regulatory functions of IL-10 during whipworm infections, we infected RAG1-deficient mice, which lack the adaptive immune compartment (T and B cells), with a high dose of *T. muris*. These mice developed a chronic infection with no symptoms of immunopathology *(Fig 10A and 10C)*. From day 35 to day 45 p.i., we treated the mice with an antibody blocking the IL-10Rα or an isotype as control. We observed no differences in survival, worm burdens, plasma chemistry parameters, caecal and liver pathology and bacterial translocation between both groups *(Fig 10)* indicating that cells of the innate immune compartment alone are not the drivers of immunopathology and in this setting IL-10 signalling plays no role.

Together, these findings suggest that expression of the IL-10 receptor on several immune cells types, is crucial in controlling the development of lethal liver disease due to dysbiosis and microbial translocation upon whipworm infection.

Discussion

We have shown that upon infection with whipworms, signalling by IL-10, but not IL-22 or IL-28, is crucial for the resistance to colonization by opportunistic pathogens, control of host inflammation, intestinal barrier maintenance and worm expulsion. We dissected the contribution of the IL-10 cytokine and the subunits of its cognate receptor and observed that lack of

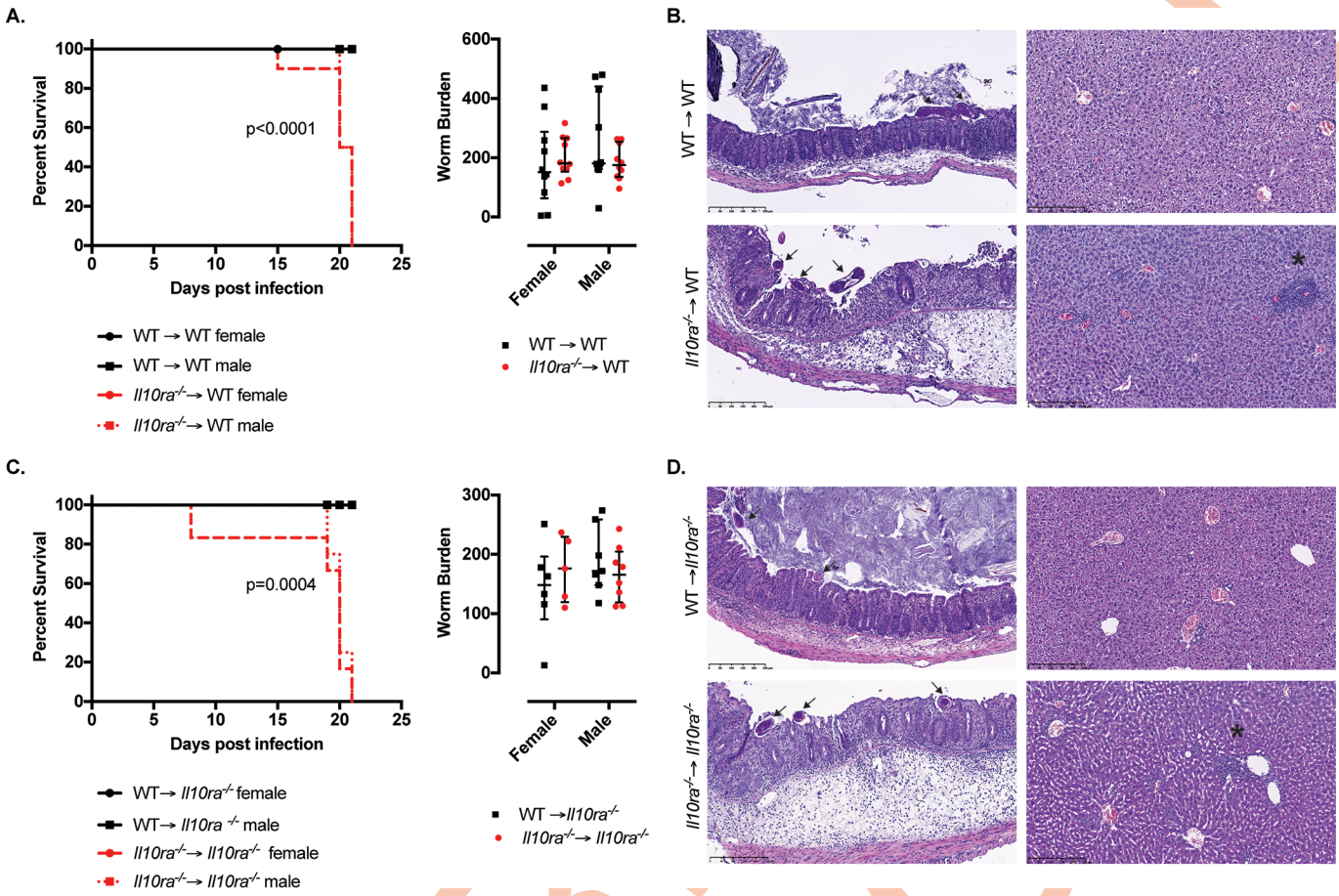

Fig 9. IL-10Rα signalling in haematopoietic cells controls immunopathology leading to reduced survival during whipworm infections. Survival curves, worm burdens and representative H&E histological images of *T. muris*-infected (high dose, 400 eggs) ten-wk-old female and male irradiated (A, B) WT and (C, D) *Il10ra*$^{-/-}$ mice reconstituted with the bone marrow of WT (black) or *Il10ra*$^{-/-}$ (red) mice. (A) Data from two independent replicas. WT → WT female n = 10. WT → WT male n = 10. *Il10ra*$^{-/-}$ → WT female n = 10. *Il10ra*$^{-/-}$ → WT male n = 10. Log-rank Mantel-Cox test for survival curves. For worm burdens, median and interquartile range are shown. (C) Data from two independent replicas. WT → *Il10ra*$^{-/-}$ female n = 6. WT → *Il10ra*$^{-/-}$ male n = 7. *Il10ra*$^{-/-}$ → *Il10ra*$^{-/-}$ female n = 6. *Il10ra*$^{-/-}$ → *Il10ra*$^{-/-}$ male n = 8. Log-rank Mantel-Cox test for survival curves. For worm burdens, median and interquartile range are shown. (B and D) *T. muris* worms infecting the mucosa are indicating with arrows and granulomatous lesions in the livers are indicated by asterisks. Scale bar, 250μm.

https://doi.org/10.1371/journal.ppat.1007265.g009

any of the components resulted in the development of a chronic whipworm infection that led to unsustainable pathology, confirming previous reports [8, 20, 21] and extending the observations to deficiency of the IL-10Rβ chain.

During whipworm infection IL-10 signalling on cells of haematopoietic origin is critical for both the development of a type-2 response resulting in worm expulsion, and the control of type-1 immunity-driven inflammation and pathology. Specifically, IL-10 promotes type-2 responses [8, 37, 38] that are indispensable for IEC turnover to maintain epithelial integrity and goblet cell hyperplasia to increase the mucus barrier. Several important roles are played by this barrier: maintaining bacterial communities that compete against and prevent colonisation by inflammatory pathobionts [39, 40]; separating IECs from luminal bacteria; and expelling the worm through the direct action of mucins [3, 41]. In contrast, the absence of IL-10 signalling results in a type-1 inflammatory response [8, 37, 38] that fails to induce the mechanisms for worm expulsion and causes intestinal epithelium damage. Inflammation and worm persistence disrupts the intestinal microbiota, affecting colonization resistance and promoting the overgrowth of opportunistic pathogens. The disruption of the epithelial barrier allows these

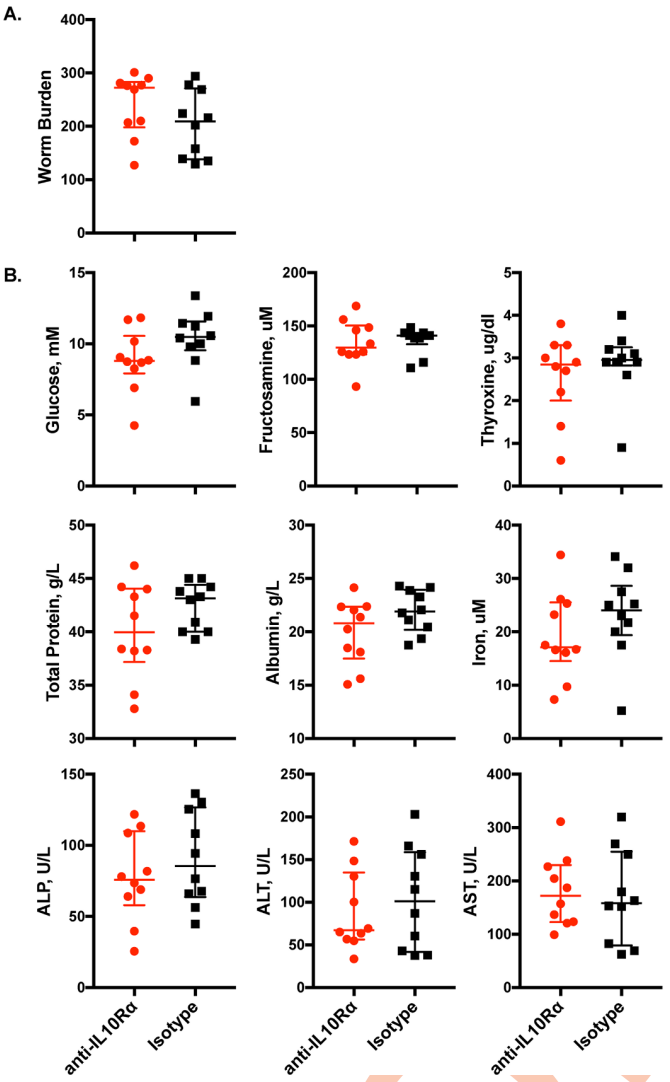

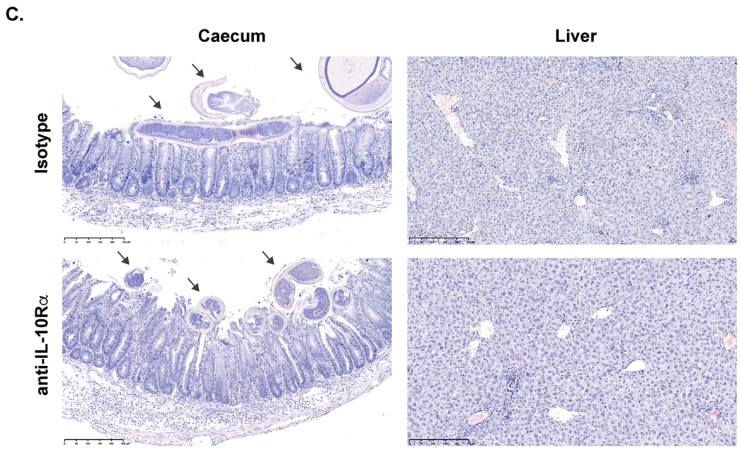

D.

		anti-IL10ra		Isotype	
Experiment		A	B	A	B
Number of mice		5	5	5	5
Family	**Species**				
Number of isolates sequenced		10	7	7	8
Enterococcaceae	*Enterococcus faecalis*	**1**	**3**		**2**
	Enterococcus gallinarum			**1**	
Enterobacteriaceae	*Escherichia coli*	**4**	**2**	**2**	**2**
Staphylococcaceae	*Staphylococcus nepalensis*	1	2	1	3
	Staphylococcus cohnii	2		3	1
	Staphylococcus lentus	1			
	Staphylococcus silvestris	1			

Fig 10. Adaptive immune cells are the main drivers of immunopathology in absence of IL-10 signalling during whipworm infections. (A) Worm burdens, (B) plasma chemistry parameters, (C) representative images of caecal and liver histological sections stained with H&E and (D) bacterial isolates from non-selective culture media of the liver of *T. muris*-infected (high dose, 400 eggs) six-wk-old female RAG1-mice treated with anti-IL10Rα and isotype control from day 35 to 45 p.i. Data from two independent replicas with similar outcome. anti-IL10Rα n = 10. Isotype n = 10. For worm burdens and plasma chemistry parameters median and interquartile range are shown. Mann Whitney U Test comparing both groups was not significant. In both groups, villous hyperplasia and *T. muris* worms infecting the mucosa (arrows) are observed in the absence of inflammation. Scale bar, 250μm. Bacterial isolates were profiled by 16S rRNA gene sequencing. *Species: the closest match by 16S rRNA gene sequence identity (> 97%).

https://doi.org/10.1371/journal.ppat.1007265.g010

pathobionts or their products to translocate and reach the liver, where they cause inflammation and necrosis resulting in liver failure and leading to lethal disease (*Fig 11*).

The actions of IL-10 signalling on the control of type-2 and -1 responses during whipworm infections may depend on the timing, cell type and organ where IL-10 is produced and the receptor is expressed. Early in an infection (before day 15 p.i.), IL-10 signalling-deficient mice, infected with *T. muris*, lacked the type-2 response and goblet cell hyperplasia observed in WT mice [37, 38]. IL-10 signalling therefore contributes to worm resistance via development of type-2 responses in the caecum and mesenteric lymph nodes, ultimately resulting in worm expulsion in WT mice. At later stages of infection (day 21–28 p.i.), IL-10 signalling controls the type-1 driven pathology both in the caecum and the liver leading to reduced survival. At

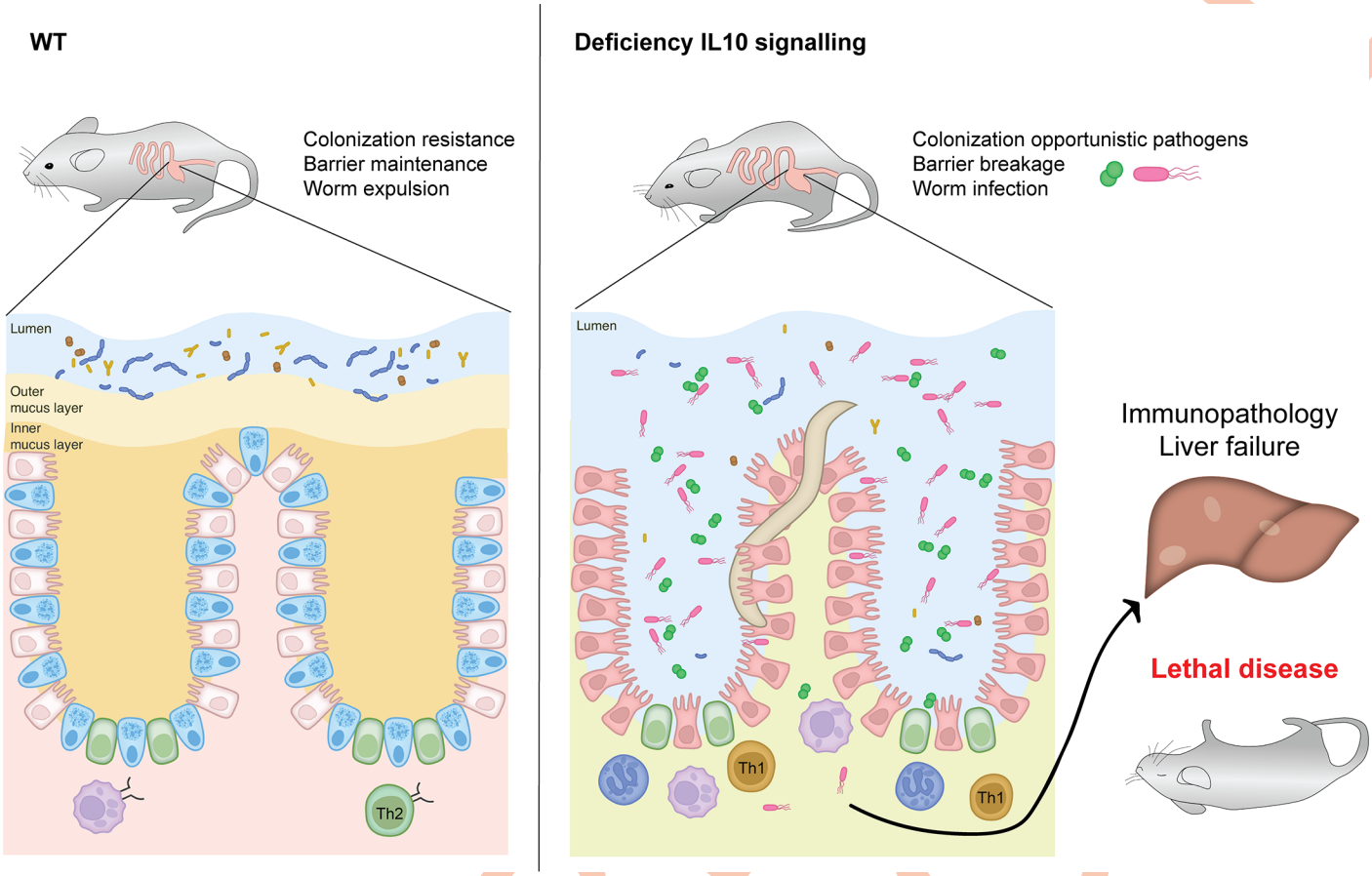

Fig 11. Mechanistic model of effects of IL-10 signalling during whipworm infections. During whipworm infection IL-10 signalling on cells of haematopoietic origin is critical for both, the development of a type-2 response resulting in worm expulsion, and the control of type-1 immunity driven immunopathology. Type-2 responses promoted by IL-10 are indispensable for the maintenance of the epithelium integrity through IEC turnover and goblet cell hyperplasia resulting in an increased mucus barrier that promotes colonization resistance, separates IECs from luminal bacteria and results in worm expulsion. Conversely, the absence of IL-10 signalling results in a type-1 inflammatory response that fails to induce the mechanisms required to expel the worm and causes intestinal epithelium damage. Inflammation and worm persistence disrupt the intestinal microbiota promoting colonization by opportunistic pathogens. The breakage of the epithelial barrier allows these pathobionts or their products to translocate and reach the liver, where they cause inflammation and necrosis resulting in liver failure and leading to lethal disease.

https://doi.org/10.1371/journal.ppat.1007265.g011

this time point, infected IL-10 signalling-deficient mice displayed higher levels of IFN-γ, IL-12, TNF-α and IL-17 and severe caecal and liver inflammation when compared with WT mice [8, 37]. Also treatment of chronically infected (low dose) WT mice after day 30 p.i. with a monoclonal antibody against IL-10R resulted in increased pathology and weight loss accompanied with increased production of type-1 cytokines [6].

Our results clearly demonstrate the haematopoietic origin of the cells that respond to IL-10 upon *T. muris* infection. In previous studies, IL-10Rα conditionally knocked out in mouse T cells, monocytes, macrophages and neutrophils did not result in inflammation or defects in worm expulsion [21]. These immune cell types alone are clearly not the main responders to IL-10. Our findings in RAG1-deficient mice indicate that cells of the innate immune compartment alone are not the drivers of immunopathology and there is no immunoregulation in these mice by IL-10. A remarkable observation is that extensive mechanical damage caused by the worm in the absence of adaptive immunity is insufficient to cause liver disease. This suggest that the immunopathology only develops in the presence of an adaptive immune system.

Our findings highlight the complexity of the IL-10 immunoregulatory response and suggest that more than one cell type may be required to respond to IL-10 at different stages during infection.

Future studies including rescue experiments transferring defined populations of IL-10R competent cells in IL-10 signalling-deficient mice or using inducible conditional knockout mice at different times during infection will help to identify the critical IL-10 responsive cell (s). The IL-10-responding cells may be stimulated directly by the microbiota or whipworms, through pattern recognition receptors such as MyD88 [42], Nod2 [39] and Nlrp6 [43] or indirectly, by limiting the inflammatory responses of other cells.

Our findings are in agreement with the multi-hit model of inflammatory gut disease [44]: infection with whipworms is a colitogenic trigger that initiates the inflammatory process; lack of IL-10 signalling causes an inflammatory type-1 response that determines the dysregulation of the mucosal immune response; and the microbiota impacts the susceptibility and responses to infection. The dysbiosis that we observed during *T. muris* infections of mice lacking IL-10 or its receptor was characterized by an increase in the abundance of opportunistic pathogens from the *Enterobacteriaceae* family *(Escherichia/Shigella)* and *Enterococcus* genus. These facultative anaerobes occur in much lower levels in the microbiota than obligate anaerobes [45]. However, host-mediated inflammation resulting from an infection or genetic predisposition, such as mutations in IL-10 [32, 36, 46, 47], increases available oxygen. The higher oxygen tension benefits the growth of aerotolerant bacteria [35, 36], disrupting the intestinal microbiota and colonization resistance [32, 36, 46, 47]. Mice deficient in IL-10 signalling do not develop spontaneous inflammation and dysbiosis in our facility. Therefore, changes to the microbiota are directly attributable to the colonization of the intestine by whipworms. We did not observe transfer of microbiota by coprophagy (in particularly, members of the *Enterobacteriaceae* family and the *Enterococcus* genus) and subsequent colitis susceptibility in co-housed uninfected and infected mice of both WT and mutant strains. Similarly, no transfer of microbiota was observed in IL-10 mutant mice co-housed with $Il10^{-/-}Nlrp6^{-/-}$ mice harbouring an expanded population of the pathobiont *Akkermansia muciniphila [43]*. Together, these results suggest that deficiency in IL-10 signalling alone is insufficient to trigger dysbiosis; whipworm infection is required to reach this disbalanced state.

We did not observe major changes to the microbiota in WT mice that cleared whipworm infections before d15 p.i. [48]. Nevertheless, the microbial alterations detected in IL-10 signalling-deficient mice, which develop chronic infections from a high-dose inoculum, were similar to those of chronically infected (low-dose) WT mice. These changes included decreased alpha diversity of the microbiota concomitantly with an increase in the abundances of *Lactobacillus* and *Enterobacteriaceae (Escherichia/Shigella)* [49, 50] and *Enterococcus* [49]. The changes in the microbiota seen during whipworm chronic infection are therefore conserved and occur more rapidly and drastically when type-1 immune responses are not regulated.

Increased abundance of *Lactobacillus* and *Enterobacteriaceae* has been also observed in the intestinal microbiota of *Heligmosomoides polygyrus*-infected susceptible mice [51, 52], and may indicate that helminth infections favour the establishment of certain bacterial groups and vice versa [49, 51, 53]. The significant reduction of bacteria of the genus *Mucispirillum* (family *Deferribacteraceae*) in the microbiota of whipworm-infected IL-10 signalling-deficient mice, is likely a consequence of the goblet cell loss, as these bacteria colonise the mucin layer of the gut [54]; indeed, *Mucispirillum* abundance increases during *Trichuris* infection of both pigs and mice [49, 50, 55], where goblet cell hyperplasia occurs.

Both *Enterobacteriaceae (Escherichia/Shigella)* and members of the *Enterococcus* genus such as *E. faecalis* are pathobionts that can cause sepsis-like disease when intestinal homeostasis is disrupted [32, 34, 35]. In whipworm-infected IL-10 signalling-deficient mice, we observed

infiltration of neutrophils and macrophages in the intestinal epithelia and neutrophilic exudates in the lumen, potentially as a mechanism of clearance of these bacteria. Nevertheless, this inflammatory response results in tissue damage and bacteriolysis that induce immunopathology [56]. Tissue damage caused by the worm further increases inflammation and opens a door for opportunistic pathogens and their products to translocate through the intestinal epithelia. When immune cells (neutrophils and macrophages) fail to control the bacteria or their products in the intestine, these are drained by the portal vein into the liver [57–59]. Liver Kupffer cells located in the periportal area phagocytise antigens and microorganisms within the portal venous circulation [57–59] and promote anti-inflammatory responses mediated in part by IL-10 [57]. Lack of IL-10 signalling and translocation of opportunistic pathogens and their products to the liver may contribute to granulomatous inflammation and production of proinflammatory cytokines by Kupffer cells and infiltrating bone-marrow-derived-monocytes/macrophages resulting in failure of microbial clearance, tissue damage with consequent liver failure [58, 59] and lethal disease. We were able to isolate *E. coli*, *E. faecalis* and *E. gallinarum* from the livers of some mutant mice and also observed increased abundances of *Enterococcus* and *Escherichia/Shigella* 16S rRNA sequences in the livers of infected IL-10Rα mutant mice. Besides bacterial growth, liver pathology and disease could also be caused by bacterial metabolites and products such as LPS of Gram-negative bacteria and lipoteichoic acid (LTA) of Gram-positive bacteria, which are known triggers of sepsis [60].

Similarly, microbial translocation has been described during hookworm [61] and HIV [62] infections that result in intestinal epithelial damage and permeability. Moreover, microbial translocation also occurs during inflammatory bowel disease (IBD) [63–65], where intestinal inflammation and damaged barrier function results from a combination of factors, including dysbiosis and mutations in genes encoding proteins involved in the immune response, such as IL-10 [57]. We did not detect LPS in serum of whipworm-infected IL-10 signalling-deficient mice (with values below the sensitivity threshold of the assay), suggesting that either the pathobionts mediating the disease are Gram-positive and therefore, other microbial products, such as LTA and peptidoglycan, may be the cause of systemic immunopathology or that opportunistic pathogens and their products were confined to the liver where they cause liver failure and disease. Previous publications showing prolonged survival of whipworm infected IL-10-deficient mice conferred by antibiotic treatment clearly support the role of microbial translocation on liver pathology and lethal disease observed in these mice [8,20]. Nevertheless, our findings on RAG1-deficient mice showing bacterial translocation in the majority of the mice in the absence of pathology suggest that microbial translocation alone is not the cause of immunopathology, but requires the presence of the adaptive immune system to trigger tissue damage.

Liver damage was reflected in changes in plasma chemistry parameters in whipworm-infected IL-10 signalling-deficient mice. Specifically, decreased hepatic synthetic function (lower plasma albumin, hypoglycaemia) and release of liver aminotransferases into the circulation are the result of hepatocyte damage and liver necrosis [66, 67]. Low albumin and enhanced cellular uptake of thyroxine by phagocytic cells results in hypothyroidism [68–70]. Low circulating levels thyroxine are related to decreased alkaline phosphatase [71] and augmented low density lipoprotein (LDL) [69]. In phagocytic cells, thyroxine increases phagocytosis, bacterial killing and TNF-α and IL-6 production [72]. Furthermore, TNF-α and IL-6 impact redistribution of iron from plasma into the liver and mononuclear phagocyte system, resulting in low concentration of plasma iron (hypoferremia) [73]. During infection, hypoferremia limits iron availability to pathogenic microorganisms and reduces the potential pro-oxidant properties of iron, which may exacerbate tissue damage [73, 74]. These changes were

reflected by increased levels of the iron binding and transport proteins, ferritin and transferrin, which are indicators of liver disease, inflammation and infection [74].

While IL-10 signalling is critical in controlling microbiota homeostasis and gut and liver immunopathology during whipworm infections, our data indicated that IL-22 is dispensable in the responses to *T. muris*. Interestingly, in our facility IL-22Rα-deficient mice infected with *C. rodentium* presented similar dysbiosis and sepsis-like pathology (caused by *E. faecalis*) to the one observed in whipworm-infected IL-10 signalling-deficient mice [32]. This may indicate that the intestinal inflammation elicited by *C. rodentium* infection of the epithelium is enough to trigger dysbiosis upon genetic predisposition by the lack of the IL22ra, while the colonization of the intestinal epithelium of these mice by whipworms is not sufficient to trigger the inflammatory responses that cause breakage of the microbiota homeostasis. In addition, the damage of the epithelium upon whipworm infection is restricted to specific areas where the worm is invading unlike *C. rodentium* infection which tends to occur more extensively across the epithelium. Moreover, the effect of IL-22 on anti-microbial production may be more relevant in responses to prokaryotic infections, such as those by *C. rodentium*.

Our results on the role of IL-22 signalling during *T. muris* infection are contrary to a previous report describing a delay in worm expulsion in IL-22 mutant mice due to reduced goblet cell hyperplasia [22]. We hypothesize this difference is due to differences in the kinetics of infection and the microbiota between mouse facilities that clearly affect the epithelial and immune intestinal responses responsible for the expulsion of the worms. Moreover, the microbiota composition of IL-22 mutant mice of each facility is directly influenced by the lack of IL-22 through its effects on antimicrobial production and mucus barrier function and this in turn affects the development of the intestinal immune system [75]. Although a role of IL-22 in inducing goblet cell hyperplasia and promoting microbiota homeostasis during whipworm infections cannot be excluded [76, 77], the induction of this mechanism of worm expulsion in the *T. muris* model is strongly dependent on the actions of IL-13 [3, 7] and regulated by IL-10 [38]. Similar observations have been made for other helminth infections in rodents including, *Nippostrongylus brasiliensis* [78] and *Hymenolepis diminuta* infections [79]. Taken together these observations suggest that in helminth infections IL-22 signalling plays a relatively minor role in worm expulsion.

Recent work has suggested that IL-28 plays a protective role in both dextran sulphate sodium and oxazalone-induced colitis in mice [80]. Our data, however, indicates that this cytokine is dispensable in responses to whipworm and consolidates the view that regulation of damage to intestinal tissue is context dependent reflecting extent of epithelial disruption. For whipworm, the data suggests that the focal damage generated by infection only becomes a significant problem in the absence of IL-10 signalling and/or following very heavy infections. Indeed, opportunistic bacteria-driven disease can occur upon heavy *T. suis* infection of weaning pigs. The resulting necrotic proliferative colitis involves crypt destruction, with inflammatory cells in the lamina propria and loss of goblet cells, and was reduced by antibiotic treatment, implicating enteric bacteria in the disease etiology [81]. Similar to our findings, accumulation of bacteria invading the mucosa was observed at the site of worm attachment and opportunistic members of the *Enterobacteriaceae* family that included *Campylobacter jejuni* and *E. coli* were isolated from these pigs and potentially contributed to the development of severe intestinal pathology [81]. Moreover, heavy *T. trichiura* infections in children cause *Trichuris* dysentery syndrome that is accompanied by a chronic inflammatory response, evidenced by high circulating levels of TNF-α [82, 83], which can potentially be driven by the overgrowth of opportunistic pathogens of the microbiota. Dysfunction of IL-10 signalling may trigger the development of dysbiosis and pathology during whipworm infection of weaning pigs and children as polymorphisms in the IL-10 gene in humans have been associated with *T.*

trichiura infection [84]. Here, the IL-10 signalling deficient mice serve as a model to understand how polymorphisms in either the cytokine or the receptor impact the responses to whipworm infections.

In summary, our data provide critical insights into how IL-10 signalling, but not IL-22 or IL-28, orchestrates protective immune responses that result in whipworm expulsion while maintaining intestinal microbial homeostasis and barrier integrity. These findings contribute to the understanding on how IL-10 signalling controls colitis during trichuriasis and on the actions of *Trichuris* ova-based therapies for diseases such as IBD. Further studies will shed light into specific immune populations driving this process through IL-10 production and exerting effector functions in response to its signalling.

Supporting information

S1 Fig. IL-10 family of cytokines and their receptors. Schematic illustration showing IL-10 family of cytokines that share the IL-10Rβ chain as a subunit of their receptors. Highlighted in bold are the molecules for which mutant mice were available and used for experiments.
(TIF)

S2 Fig. IL-22 and IL-28 signalling are dispensable in responses to high dose *T. muris* infections. Antibody (IgG1 and IgG2a/c) titres of *T. muris*-infected, six to ten-wk-old female WT and **(A)** *Il22*$^{-/-}$, **(B)** *Il22ra*$^{-/-}$ and **(C)** *Il28ra*$^{-/-}$ mice after 32 days of high dose infection (400 eggs). No differences in worm expulsion were observed at this time point. Data from two independent replicas. Median and interquartile range are shown. **(A)** WT n = 12, *Il22*$^{-/-}$ n = 13. **(B)** WT n = 14, *Il22ra*$^{-/-}$ n = 18. **(C)** WT n = 12, *Il28ra*$^{-/-}$ n = 12.
(TIF)

S3 Fig. IL-22 and IL-28 signalling are dispensable in responses to high dose *T. muris* infections. Antibody (IgG1 and IgG2a/c) titres of *T. muris*-infected, six to ten-wk-old female WT and **(A)** *Il22*$^{-/-}$, **(B)** *Il22ra*$^{-/-}$ and **(C)** *Il28ra*$^{-/-}$ mice after 21 days of high dose infection (400 eggs). No differences in worm expulsion were observed at this time point. Data from two independent replicas. Median and interquartile range are shown. **(A)** WT n = 13, *Il22*$^{-/-}$ n = 13. **(B)** WT n = 13, *Il22ra*$^{-/-}$ n = 14. **(C)** WT n = 12, *Il28ra*$^{-/-}$ n = 12.
(TIF)

S4 Fig. IL-22 and IL-28 signalling are dispensable in responses to low dose *T. muris* infections. Worm burden and antibody (IgG1 and IgG2a/c) titres of *T. muris*-infected, six to ten-wk-old female WT and **(A)** *Il22*$^{-/-}$, **(B)** *Il22ra*$^{-/-}$ and **(C)** *Il28ra*$^{-/-}$ mice after 35 days of low dose infection (20–25 eggs). Data from two independent replicas. Median and interquartile range are shown. **(A)** WT n = 12, *Il22*$^{-/-}$ n = 13. **(B)** WT n = 12, *Il22ra*$^{-/-}$ n = 11. **(C)** WT n = 12, *Il28ra*$^{-/-}$ n = 13.
(TIF)

S5 Fig. Whipworm infection of IL-10 signalling-deficient mice results in loss of goblet cells in caecal epithelium. Representative images of PAS staining on caecum sections of *T. muris*-infected (high dose, 400 eggs) **(A)** WT, **(B)** *Il10*$^{-/-}$, **C)** *Il10ra*$^{-/-}$ and **(D)** *Il10rb*$^{-/-}$ mice upon culling. Infected WT mice present goblet cell hyperplasia while infected IL-10 signalling-deficient mice show goblet cell loss. *T. muris* worms are infecting the mucosa (arrows) of IL-10 signalling-deficient mice. Scale bar, 250μm. Data from two independent replicas (n = 5–10 each).
(TIF)

S6 Fig. Defective IL-10 signalling results in liver immunopathology characterised by foamy macrophages upon whipworm infection. Liver histopathology of uninfected and *T.*

muris-infected (high dose, 400 eggs) **(A)** WT, **(B)** *Il10*$^{-/-}$, **(C)** *Il10ra*$^{-/-}$ and **(D)** *Il10rb*$^{-/-}$ mice upon culling. Sections stained with H&E. Uninfected WT and mutant mice show no lesions. Upon infection, some IL-10 signalling-deficient mice show inflammatory infiltrate characterized by foamy macrophages. Scale bar, 50μm. Data from two independent replicas (n = 5–18 each).
(TIF)

S7 Fig. Liver disease upon defects on IL-10 signalling during *T. muris* infection is reflected in plasma chemistry changes. Percentage change of plasma chemistry parameters upon culling of *T. muris*-infected (high dose, 400 eggs), six-wk-old female and male littermate WT and **(A)** *Il10*$^{-/-}$, **(B)** *Il10ra*$^{-/-}$, **(C)** *Il10rb*$^{-/-}$ mice.
The infection status effect on each genotype for plasma chemistry parameters associated with liver disease was estimated across independent experiments. The estimate has been visualised as a percentage normalised value (signal/average signal for that parameter) along with the 95% confidence interval to allow comparison across variables. Highlighted in red, are parameters where the genotype by infection is statistically significant in explaining variation after adjustment for multiple testing (5% FDR) and are significant in the final model estimate ($p<0.05$).
(A) Data from three independent replicas. WT n = 24. *Il10*$^{-/-}$ n = 23.
(B) Data from three independent replicas. WT n = 25. *Il10ra*$^{-/-}$ n = 22.
(C) Data from two independent replicas. WT n = 16. *Il10rb*$^{-/-}$ n = 18.
Alkaline phosphatase (Alp), aspartate aminotransferase (Ast), alanine aminotransferase (Alt)), glucose (Gluc), fructosamine (Fruct), total protein (Tp), albumin (Alb), thyroxine (Thyrx), transferrin (Tf), ferritin (Ferr), cholesterol (Chol), high density lipoprotein (Hdl), low density lipoprotein (Ldl), triglycerides (Trigs), total bilirubin (Tblic), urea, creatinine (Creat) and creatinine kinase (CK).
(TIF)

S8 Fig. Inflammatory systemic responses upon *T. muris* infection of defective IL-10 signalling mice. IL-6 and TNF-α concentrations in plasma of *T. muris*-infected (high dose, 400 eggs), six-wk-old female and male littermate WT and **(A)** *Il10*$^{-/-}$ and **(B)** *Il10rb*$^{-/-}$ mice.
(A) Data from two independent replicas. WT n = 7. *Il10*$^{-/-}$ n = 7. Median and interquartile range are shown. Mann Whitney U Test, $^{***}p<0.001$.
(B) Data from two independent replicas. WT n = 7. *Il10rb*$^{-/-}$ n = 7. Median and interquartile range are shown. Mann Whitney U Test, $^{***}p<0.001$.
(TIF)

S9 Fig. Caecal dysbiosis upon whipworm infection and defective IL-10 signalling is associated with expanded populations of pathobionts. Caecal microbial community structure at the operational taxonomic unit (OTU) level of co-housed uninfected and *T. muris*-infected (high dose, 400 eggs) six-wk-old female and male littermate WT and *Il10*$^{-/-}$ mice at day of culling. **(A)** Principal Coordinates Analysis (PCoA) and Canonical Correspondence Analysis (CCA p = 0.001), the numbers in bracket indicate the percentage variance explained by that component. **(B)** beta-diversity index (ANOSIM R = 0.336 and p = 0.001), **(C)** alpha-diversity indexes (Shannon diversity, richness and evenness; ANOVA $p<0.001$, $p<0.001$, $p<0.001$, respectively), **(D)** network analysis, **(E)** Linear Discriminant Analysis Effect Size (LEfSe) analysis and **(F)** bar plots representing proportional abundance of individual OTUs in caecal microbial community structures. Data from two independent replicas. WT uninfected n = 9. WT infected n = 16. *Il10*$^{-/-}$ uninfected n = 6. *Il10*$^{-/-}$ infected n = 15.
(TIF)

S10 Fig. Caecal dysbiosis upon whipworm infection and defective IL-10Rα signalling is associated with expanded populations of pathobionts. Caecal microbial community structure at the operational taxonomic unit (OTU) level of co-housed uninfected and *T. muris*-infected (high dose, 400 eggs) six-wk-old female and male littermate WT and *Il10ra*$^{-/-}$ mice at day of culling. **(A)** Principal Coordinates Analysis (PCoA) and Canonical Correspondence Analysis (CCA p = 0.001), the numbers in bracket indicate the percentage variance explained by that component. **(B)** beta-diversity index (ANOSIM R = 0.347 and p = 0.001), **(C)** alpha-diversity indexes (Shannon diversity, richness and evenness; ANOVA p = 0.003, p<0.001, p<0.001, respectively), **(D)** network analysis, **(E)** Linear Discriminant Analysis Effect Size (LEfSe) analysis and **(F)** bar plots representing proportional abundance of individual OTUs in caecal microbial community structures. Data from two independent replicas. WT uninfected n = 6. WT infected n = 19. *Il10ra*$^{-/-}$ uninfected n = 11. *Il10ra*$^{-/-}$ infected n = 16.
(TIF)

S11 Fig. Caecal dysbiosis upon whipworm infection and defective IL-10Rβ signalling is associated with expanded populations of pathobionts. Caecal microbial community structure at the operational taxonomic unit (OTU) level of co-housed uninfected and *T. muris*-infected (high dose, 400 eggs) six-wk-old female and male littermate WT and *Il10rb*$^{-/-}$ mice at day of culling. **(A)** Principal Coordinates Analysis (PCoA) and Canonical Correspondence Analysis (CCA p = 0.001), the numbers in bracket indicate the percentage variance explained by that component. **(B)** beta-diversity index (ANOSIM R = 0.239 and p = 0.001), **(C)** alpha-diversity indexes (Shannon diversity, richness and evenness; ANOVA p = 0.03, p<0.001, p<0.001, respectively), **(D)** network analysis, **(E)** Linear Discriminant Analysis Effect Size (LEfSe) analysis and **(F)** bar plots representing proportional abundance of individual OTUs in caecal microbial community structures. Data from two independent replicas. WT uninfected n = 15. WT infected n = 16. *Il10rb*$^{-/-}$ uninfected n = 17. *Il10rb*$^{-/-}$ infected n = 19.
(TIF)

S12 Fig. Extend of microbiota colonization by pathobionts correlates with reduced survival and liver disease of whipworm-infected IL-10 signalling-deficient mice. (A) The degree of colonization by *Enterococcus* and *Enterobacteriaceae* (percentage of abundance from total microbiota) among IL-10 signalling-deficient mice showing a severe or mild phenotype upon whipworm infection was compared. A severe phenotype is characterised by presence of granulomas, necrosis and foamy macrophages in the liver, weight loss and poor survival. A mild phenotype involves minor liver infiltration, no weight loss and extended survival. For percentage of *Enterococcus* and *Enterobacteriaceae* (including *Escherichia-Shigella*), median and interquartile range are shown. Mann Whitney U Test, $^{**}p<0.005$, $^{*}p = 0.05$.
(B) Correlation analysis of the degree of colonization of the pathobionts and the plasma levels of the liver enzyme aspartate aminotransferase (Ast) was performed using a two-tailed Spearman correlation test with a 95% confidence interval. r, Spearman's rank correlation coefficient.
Data from two independent replicas. n = 4–11 each group.
(TIF)

S13 Fig. IL-10Rβ signalling in haematopoietic cells is essential to control immunopathology leading to reduced survival during whipworm infections. Survival curves, worm burdens and representative H&E histological images of *T. muris*-infected (high dose, 400 eggs) ten-wk-old female and male irradiated **(A, B)** WT and **(C, D)** *Il10rb*$^{-/-}$ mice reconstituted with the bone marrow of WT (black) or *Il10rb*$^{-/-}$ (red) mice.
(A) Data from two independent replicas. WT → WT female n = 10. WT → WT male n = 10.

Il10rb$^{-/-}$ → WT female n = 10. *Il10rb*$^{-/-}$ → WT male n = 10. For worm burdens, median and interquartile range are shown. Log-rank Mantel-Cox test for survival curves.
(B) Data from two independent replicas. WT → *Il10rb*$^{-/-}$ female n = 7. WT → *Il10rb*$^{-/-}$ male n = 5. *Il10rb*$^{-/-}$ → *Il10rb*$^{-/-}$ female n = 5. *Il10rb*$^{-/-}$ → *Il10rb*$^{-/-}$ male n = 6. For worm burdens, median and interquartile range are shown. Log-rank Mantel-Cox test for survival curves.
(B and D) *T. muris* worms infecting the mucosa are indicating with arrows and granulomatous lesions in the livers are indicated by asterisks. Scale bar, 250μm.
(TIF)

S14 Fig. Lack of IL-10Ra on IECs does not impact worm expulsion and immune responses during *T. muris* infections. Antibody (IgG1, IgG2a/c and IgE) titers of *T. muris*-infected (high dose, 400 eggs) six-wk-old female and male littermates *Il10ra*$^{+/+}$ *Vil*$^{cre/+}$, *Il10ra*$^{fl/fl}$ *Vil*$^{+/+}$ and *Il10ra*$^{fl/fl}$ *Vil*$^{cre/+}$ mice after **(A)** 20 days (n = 16 mice for each group) and **(B)** 32 days of infection (n = 14 mice for each group). Data from two independent replicas. Median and interquartile range are shown.
(TIF)

S1 File. Supplemental Experimental Procedures. Extended information on housing and husbandry of mice and microbiota analysis is provided in this file.
(DOCX)

S2 File. 3i consortium authors. List of The 3i consortium authors and their affiliations.
(XLSX)

S1 Table. Integrated Data Analysis estimates of the effect of genotype (WT or *Il10*$^{-/-}$) after accounting for infection on plasma chemistry parameters. The effect of genotype on plasma chemistry parameters for both infected and non-infected animals was explored using an Integrated Data Analysis. A complex regression model was fitted to account for various sources of variation including genotype, sex and infection status. The model also includes interaction terms between these elements. From this model, we can therefore isolate the impact of genotype on the plasma variables both as a main effect and as an effect interacting with sex. The estimates for these elements of the model is captured in the table and include the significance of these terms as assessed by a F-test and after adjustment for multiple testing to control the false discovery rate to 5% (Benjamin and Hochberg method). Est (Estimate), SE (Standard Error), pVal (p value), Sig (significant).
(XLSX)

S2 Table. Integrated Data Analysis estimates of the effect of genotype (WT or *Il10ra*$^{-/-}$) after accounting for infection on plasma chemistry parameters. The effect of genotype on plasma chemistry parameters for both infected and non-infected animals was explored using an Integrated Data Analysis. A complex regression model was fitted to account for various sources of variation including genotype, sex and infection status. The model also includes interaction terms between these elements. From this model, we can therefore isolate the impact of genotype on the plasma variables both as a main effect and as an effect interacting with sex. The estimates for these elements of the model is captured in the table and include the significance of these terms as assessed by a F-test and after adjustment for multiple testing to control the false discovery rate to 5% (Benjamin and Hochberg method). Est (Estimate), SE (Standard Error), pVal (p value), Sig (significant).
(XLSX)

S3 Table. Integrated Data Analysis estimates of the effect of genotype (WT or *Il10rb*$^{-/-}$) after accounting for infection on plasma chemistry parameters. The effect of genotype on

plasma chemistry parameters for both infected and non-infected animals was explored using an Integrated Data Analysis. A complex regression model was fitted to account for various sources of variation including genotype, sex and infection status. The model also includes interaction terms between these elements. From this model, we can therefore isolate the impact of genotype on the plasma variables both as a main effect and as an effect interacting with sex. The estimates for these elements of the model is captured in the table and include the significance of these terms as assessed by a F-test and after adjustment for multiple testing to control the false discovery rate to 5% (Benjamin and Hochberg method). Est (Estimate), SE (Standard Error), pVal (p value), Sig (significant).
(XLSX)

S4 Table. Integrated Data Analysis estimates of the effect of genotype (WT or KO) as a function of infection on plasma chemistry parameters. The effect of genotype on plasma chemistry parameters for both infected and non-infected animals was explored using an Integrated Data Analysis. A complex regression model was fitted to account for various sources of variation including genotype, sex and infection status. The model also includes interaction terms between these elements. From this model, we can therefore isolate the impact of genotype with infection on the plasma variables. The estimates for these elements of the model is captured in the table and include the significance of these terms as assessed by a F-test and after adjustment for multiple testing to control the false discovery rate to 5% (Benjamin and Hochberg method). Est (Estimate), SE (Standard Error), pVal (p value), Sig (significant).
(XLS)

S5 Table. Isolation and identification by 16S rRNA gene sequencing of systemic bacterial isolates in *T. muris*-infected WT and *Il10*$^{-/-}$ mice. A-E indicate independent experiments with similar outcome. In each experiment, *Il10*$^{-/-}$ animals showing significant signs of morbidity were examined for bacterial breakthrough in the livers. Isolates from non-selective culture media were profiled by 16S rRNA gene sequencing. *Species: the closest match by 16S rRNA gene sequence identity (> 97%).
(XLSX)

S6 Table. Isolation and identification by 16S rRNA gene sequencing of systemic bacterial isolates in *T. muris*-infected WT and *Il10ra*$^{-/-}$ mice. A-E indicate independent experiments with similar outcome. In each experiment, *Il10ra*$^{-/-}$ animals showing significant signs of morbidity were examined for bacterial breakthrough in the livers. Isolates from non-selective culture media were profiled by 16S rRNA gene sequencing. *Species: the closest match by 16S rRNA gene sequence identity (> 97%).
(XLSX)

S7 Table. Isolation and identification by 16S rRNA gene sequencing of systemic bacterial isolates in *T. muris*-infected WT and *Il10rb*$^{-/-}$ mice. A-E indicate independent experiments with similar outcome. In each experiment, *Il10rb*$^{-/-}$ animals showing significant signs of morbidity were examined for bacterial breakthrough in the livers. Isolates from non-selective culture media were profiled by 16S rRNA gene sequencing. *Species: the closest match by 16S rRNA gene sequence identity (> 97%).
(XLSX)

Acknowledgments

We are grateful to S. Clare, C. Brandt and G. Notley for assistance with mouse experiments; E. Ryder for genotyping; A. Kirton and H. Wardle-Jones for mouse colony breeding; T. D.

Lawley, H. Browne and N. Kumar for microbiota analysis and interpretation; S. Thompson for histology scoring; and M. Sanders for assistance in sequencing. We thank Jose A. Dianes-Santos for design of graphic illustrations.

Author Contributions

Conceptualization: María A. Duque-Correa, Natasha A. Karp, Gordon Dougan, Richard K. Grencis, Matthew Berriman.

Data curation: María A. Duque-Correa, Natasha A. Karp, Timothy P. Jenkins, Adam J. Reid, Emma L. Cambridge.

Formal analysis: María A. Duque-Correa, Natasha A. Karp, Timothy P. Jenkins, Adam J. Reid.

Funding acquisition: María A. Duque-Correa, Gordon Dougan, Richard K. Grencis, Matthew Berriman.

Investigation: María A. Duque-Correa, Catherine McCarthy, Simon Forman, David Goulding, Geetha Sankaranarayanan, Emma L. Cambridge, Carmen Ballesteros Reviriego.

Methodology: María A. Duque-Correa, Natasha A. Karp, Richard K. Grencis, Matthew Berriman.

Project administration: María A. Duque-Correa.

Resources: Werner Müller, Gordon Dougan, Richard K. Grencis, Matthew Berriman.

Supervision: Gordon Dougan, Richard K. Grencis, Matthew Berriman.

Validation: María A. Duque-Correa.

Visualization: María A. Duque-Correa, Natasha A. Karp, David Goulding, Timothy P. Jenkins, Adam J. Reid.

Writing – original draft: María A. Duque-Correa, Natasha A. Karp, Timothy P. Jenkins, Adam J. Reid, Cinzia Cantacessi, Richard K. Grencis, Matthew Berriman.

Writing – review & editing: María A. Duque-Correa, Natasha A. Karp, Timothy P. Jenkins, Adam J. Reid, Cinzia Cantacessi, Richard K. Grencis, Matthew Berriman.

References

1. Peterson LW, Artis D. Intestinal epithelial cells: regulators of barrier function and immune homeostasis. Nature reviews Immunology. 2014; 14(3):141–53. https://doi.org/10.1038/nri3608 PMID: 24566914
2. Artis D, Grencis RK. The intestinal epithelium: sensors to effectors in nematode infection. Mucosal immunology. 2008; 1(4):252–64. https://doi.org/10.1038/mi.2008.21 PMID: 19079187
3. Grencis RK. Immunity to helminths: resistance, regulation, and susceptibility to gastrointestinal nematodes. Annu Rev Immunol. 2015; 33:201–25. https://doi.org/10.1146/annurev-immunol-032713-120218 PMID: 25533702
4. Bethony J, Brooker S, Albonico M, Geiger SM, Loukas A, Diemert D, et al. Soil-transmitted helminth infections: ascariasis, trichuriasis, and hookworm. Lancet. 2006; 367(9521):1521–32. https://doi.org/10.1016/S0140-6736(06)68653-4 PMID: 16679166
5. WHO. Eliminating soil-transmitted helminthiases as a public health problem in children: Progress report 2001–2010 and strategic plan 2011–2020. Available: http://whqlibdocwhoint/publications/2012/9789241503129_engpdf?ua=1.2013.
6. Grencis RK, Humphreys NE, Bancroft AJ. Immunity to gastrointestinal nematodes: mechanisms and myths. Immunological reviews. 2014; 260(1):183–205. https://doi.org/10.1111/imr.12188 PMID: 24942690

7. Klementowicz JE, Travis MA, Grencis RK. Trichuris muris: a model of gastrointestinal parasite infection. Seminars in immunopathology. 2012; 34(6):815–28. https://doi.org/10.1007/s00281-012-0348-2 PMID: 23053395
8. Schopf LR, Hoffmann KF, Cheever AW, Urban JF Jr., Wynn TA. IL-10 is critical for host resistance and survival during gastrointestinal helminth infection. J Immunol. 2002; 168(5):2383–92. PMID: 11859129
9. Shouval DS, Ouahed J, Biswas A, Goettel JA, Horwitz BH, Klein C, et al. Interleukin 10 receptor signaling: master regulator of intestinal mucosal homeostasis in mice and humans. Adv Immunol. 2014; 122:177–210. https://doi.org/10.1016/B978-0-12-800267-4.00005-5 PMID: 24507158
10. Ouyang W, Rutz S, Crellin NK, Valdez PA, Hymowitz SG. Regulation and functions of the IL-10 family of cytokines in inflammation and disease. Annu Rev Immunol. 2011; 29:71–109. https://doi.org/10.1146/annurev-immunol-031210-101312 PMID: 21166540
11. Akdis M, Burgler S, Crameri R, Eiwegger T, Fujita H, Gomez E, et al. Interleukins, from 1 to 37, and interferon-gamma: receptors, functions, and roles in diseases. J Allergy Clin Immunol. 2011; 127 (3):701–21 e1-70. https://doi.org/10.1016/j.jaci.2010.11.050 PMID: 21377040
12. Commins S, Steinke JW, Borish L. The extended IL-10 superfamily: IL-10, IL-19, IL-20, IL-22, IL-24, IL-26, IL-28, and IL-29. J Allergy Clin Immunol. 2008; 121(5):1108–11. https://doi.org/10.1016/j.jaci.2008.02.026 PMID: 18405958
13. Kuhn R, Lohler J, Rennick D, Rajewsky K, Muller W. Interleukin-10-deficient mice develop chronic enterocolitis. Cell. 1993; 75(2):263–74. PMID: 8402911
14. Spencer SD, Di Marco F, Hooley J, Pitts-Meek S, Bauer M, Ryan AM, et al. The orphan receptor CRF2-4 is an essential subunit of the interleukin 10 receptor. J Exp Med. 1998; 187(4):571–8. PMID: 9463407
15. Sabat R, Ouyang W, Wolk K. Therapeutic opportunities of the IL-22-IL-22R1 system. Nat Rev Drug Discov. 2014; 13(1):21–38. https://doi.org/10.1038/nrd4176 PMID: 24378801
16. Egli A, Santer DM, O'Shea D, Tyrrell DL, Houghton M. The impact of the interferon-lambda family on the innate and adaptive immune response to viral infections. Emerg Microbes Infect. 2014; 3(7):e51. https://doi.org/10.1038/emi.2014.51 PMID: 26038748
17. Lazear HM, Nice TJ, Diamond MS. Interferon-lambda: Immune Functions at Barrier Surfaces and Beyond. Immunity. 2015; 43(1):15–28. https://doi.org/10.1016/j.immuni.2015.07.001 PMID: 26200010
18. Syedbasha M, Egli A. Interferon Lambda: Modulating Immunity in Infectious Diseases. Front Immunol. 2017; 8:119. https://doi.org/10.3389/fimmu.2017.00119 PMID: 28293236
19. Stephen-Victor E, Fickenscher H, Bayry J. IL-26: An Emerging Proinflammatory Member of the IL-10 Cytokine Family with Multifaceted Actions in Antiviral, Antimicrobial, and Autoimmune Responses. PLoS Pathog. 2016; 12(6):e1005624. https://doi.org/10.1371/journal.ppat.1005624 PMID: 27337042
20. Kopper JJ, Patterson JS, Mansfield LS. Metronidazole-but not IL-10 or prednisolone-rescues Trichuris muris infected C57BL/6 IL-10 deficient mice from severe disease. Vet Parasitol. 2015; 212(3–4):239–52. https://doi.org/10.1016/j.vetpar.2015.07.038 PMID: 26277566
21. Pils MC, Pisano F, Fasnacht N, Heinrich JM, Groebe L, Schippers A, et al. Monocytes/macrophages and/or neutrophils are the target of IL-10 in the LPS endotoxemia model. Eur J Immunol. 2010; 40 (2):443–8. https://doi.org/10.1002/eji.200939592 PMID: 19941312
22. Turner JE, Stockinger B, Helmby H. IL-22 mediates goblet cell hyperplasia and worm expulsion in intestinal helminth infection. PLoS Pathog. 2013; 9(10):e1003698. https://doi.org/10.1371/journal.ppat.1003698 PMID: 24130494
23. Kreymborg K, Etzensperger R, Dumoutier L, Haak S, Rebollo A, Buch T, et al. IL-22 is expressed by Th17 cells in an IL-23-dependent fashion, but not required for the development of autoimmune encephalomyelitis. J Immunol. 2007; 179(12):8098–104. PMID: 18056351
24. White JK, Gerdin AK, Karp NA, Ryder E, Buljan M, Bussell JN, et al. Genome-wide generation and systematic phenotyping of knockout mice reveals new roles for many genes. Cell. 2013; 154(2):452–64. https://doi.org/10.1016/j.cell.2013.06.022 PMID: 23870131
25. Wakelin D. Acquired immunity to Trichuris muris in the albino laboratory mouse. Parasitology. 1967; 57 (3):515–24. PMID: 6048569
26. Bancroft AJ, Else KJ, Humphreys NE, Grencis RK. The effect of challenge and trickle Trichuris muris infections on the polarisation of the immune response. Int J Parasitol. 2001; 31(14):1627–37. PMID: 11730790
27. Else KJ, Entwistle GM, Grencis RK. Correlations between worm burden and markers of Th1 and Th2 cell subset induction in an inbred strain of mouse infected with Trichuris muris. Parasite Immunol. 1993; 15(10):595–600. PMID: 7877836
28. Caporaso JG, Kuczynski J, Stombaugh J, Bittinger K, Bushman FD, Costello EK. QIIME allows analysis of high-throughput community sequencing data. Nature Meth. 2010; 7.

29. du Sert NP, Bamsey I, Bate ST, Berdoy M, Clark RA, Cuthill IC, et al. The Experimental Design Assistant. Nat Methods. 2017; 14(11):1024–5. https://doi.org/10.1038/nmeth.4462 PMID: 28960183

30. Curran PJ, Hussong AM. Integrative data analysis: the simultaneous analysis of multiple data sets. Psychol Methods. 2009; 14(2):81–100. https://doi.org/10.1037/a0015914 PMID: 19485623

31. Benjamini YH, Yosef Controlling the false discovery rate: a practical and powerful approach to multiple testing. Journal of the Royal Statistical Society. 1995(Series B (Methodological)):289–300.

32. Pham TA, Clare S, Goulding D, Arasteh JM, Stares MD, Browne HP, et al. Epithelial IL-22RA1-mediated fucosylation promotes intestinal colonization resistance to an opportunistic pathogen. Cell Host Microbe. 2014; 16(4):504–16. https://doi.org/10.1016/j.chom.2014.08.017 PMID: 25263220

33. Stecher B, Hardt WD. Mechanisms controlling pathogen colonization of the gut. Curr Opin Microbiol. 2011; 14(1):82–91. https://doi.org/10.1016/j.mib.2010.10.003 PMID: 21036098

34. Ayres JS, Trinidad NJ, Vance RE. Lethal inflammasome activation by a multidrug-resistant pathobiont upon antibiotic disruption of the microbiota. Nat Med. 2012; 18(5):799–806. https://doi.org/10.1038/nm.2729 PMID: 22522562

35. Levy M, Kolodziejczyk AA, Thaiss CA, Elinav E. Dysbiosis and the immune system. Nature reviews Immunology. 2017; 17(4):219–32. https://doi.org/10.1038/nri.2017.7 PMID: 28260787

36. Lupp C, Robertson ML, Wickham ME, Sekirov I, Champion OL, Gaynor EC, et al. Host-mediated inflammation disrupts the intestinal microbiota and promotes the overgrowth of Enterobacteriaceae. Cell Host Microbe. 2007; 2(3):204. PMID: 18030708

37. Fasnacht N, Greweling MC, Bollati-Fogolin M, Schippers A, Muller W. T-cell-specific deletion of gp130 renders the highly susceptible IL-10-deficient mouse resistant to intestinal nematode infection. Eur J Immunol. 2009; 39(8):2173–83. https://doi.org/10.1002/eji.200838710 PMID: 19593768

38. Wilson MS, Ramalingam TR, Rivollier A, Shenderov K, Mentink-Kane MM, Madala SK, et al. Colitis and intestinal inflammation in IL10-/- mice results from IL-13Ralpha2-mediated attenuation of IL-13 activity. Gastroenterology. 2011; 140(1):254–64. https://doi.org/10.1053/j.gastro.2010.09.047 PMID: 20951137

39. Ramanan D, Bowcutt R, Lee SC, Tang MS, Kurtz ZD, Ding Y, et al. Helminth infection promotes colonization resistance via type 2 immunity. Science. 2016; 352(6285):608–12. https://doi.org/10.1126/science.aaf3229 PMID: 27080105

40. Broadhurst MJ, Ardeshir A, Kanwar B, Mirpuri J, Gundra UM, Leung JM, et al. Therapeutic helminth infection of macaques with idiopathic chronic diarrhea alters the inflammatory signature and mucosal microbiota of the colon. PLoS Pathog. 2012; 8(11):e1003000. https://doi.org/10.1371/journal.ppat.1003000 PMID: 23166490

41. Harris NL, Loke P. Recent Advances in Type-2-Cell-Mediated Immunity: Insights from Helminth Infection. Immunity. 2017; 47(6):1024–36. https://doi.org/10.1016/j.immuni.2017.11.015 PMID: 29262347

42. Hoshi N, Schenten D, Nish SA, Walther Z, Gagliani N, Flavell RA, et al. MyD88 signalling in colonic mononuclear phagocytes drives colitis in IL-10-deficient mice. Nat Commun. 2012; 3:1120. https://doi.org/10.1038/ncomms2113 PMID: 23047678

43. Seregin SS, Golovchenko N, Schaf B, Chen J, Pudlo NA, Mitchell J, et al. NLRP6 Protects Il10(-/-) Mice from Colitis by Limiting Colonization of Akkermansia muciniphila. Cell Rep. 2017; 19(10):2174.

44. Keubler LM, Buettner M, Hager C, Bleich A. A Multihit Model: Colitis Lessons from the Interleukin-10-deficient Mouse. Inflamm Bowel Dis. 2015; 21(8):1967–75. https://doi.org/10.1097/MIB.0000000000000468 PMID: 26164667

45. Eckburg PB, Bik EM, Bernstein CN, Purdom E, Dethlefsen L, Sargent M, et al. Diversity of the human intestinal microbial flora. Science. 2005; 308(5728):1635–8. https://doi.org/10.1126/science.1110591 PMID: 15831718

46. Maharshak N, Packey CD, Ellermann M, Manick S, Siddle JP, Huh EY, et al. Altered enteric microbiota ecology in interleukin 10-deficient mice during development and progression of intestinal inflammation. Gut Microbes. 2013; 4(4):316–24. https://doi.org/10.4161/gmic.25486 PMID: 23822920

47. Stecher B, Robbiani R, Walker AW, Westendorf AM, Barthel M, Kremer M, et al. Salmonella enterica serovar typhimurium exploits inflammation to compete with the intestinal microbiota. PLoS Biol. 2007; 5(10):2177–89. https://doi.org/10.1371/journal.pbio.0050244 PMID: 17760501

48. Wakelin D. Genetic control of immune responses to parasites: immunity to Trichuris muris in inbred and random-bred strains of mice. Parasitology. 1975; 71(1):51–60. PMID: 1178220

49. Holm JB, Sorobetea D, Kiilerich P, Ramayo-Caldas Y, Estelle J, Ma T, et al. Chronic Trichuris muris Infection Decreases Diversity of the Intestinal Microbiota and Concomitantly Increases the Abundance of Lactobacilli. PLoS One. 2015; 10(5):e0125495. https://doi.org/10.1371/journal.pone.0125495 PMID: 25942314

50. Houlden A, Hayes KS, Bancroft AJ, Worthington JJ, Wang P, Grencis RK, et al. Chronic Trichuris muris Infection in C57BL/6 Mice Causes Significant Changes in Host Microbiota and Metabolome: Effects

Reversed by Pathogen Clearance. PLoS One. 2015; 10(5):e0125945. https://doi.org/10.1371/journal.pone.0125945 PMID: 25938477

51. Reynolds LA, Smith KA, Filbey KJ, Harcus Y, Hewitson JP, Redpath SA, et al. Commensal-pathogen interactions in the intestinal tract: lactobacilli promote infection with, and are promoted by, helminth parasites. Gut Microbes. 2014; 5(4):522–32. https://doi.org/10.4161/gmic.32155 PMID: 25144609

52. Rausch S, Held J, Fischer A, Heimesaat MM, Kuhl AA, Bereswill S, et al. Small intestinal nematode infection of mice is associated with increased enterobacterial loads alongside the intestinal tract. PLoS One. 2013; 8(9):e74026. https://doi.org/10.1371/journal.pone.0074026 PMID: 24040152

53. Peachey LE, Jenkins TP, Cantacessi C. This Gut Ain't Big Enough for Both of Us. Or Is It? Helminth-Microbiota Interactions in Veterinary Species. Trends Parasitol. 2017; 33(8):619–32. https://doi.org/10.1016/j.pt.2017.04.004 PMID: 28506779

54. Robertson BR, O'Rourke JL, Neilan BA, Vandamme P, On SL, Fox JG, et al. Mucispirillum schaedleri gen. nov., sp. nov., a spiral-shaped bacterium colonizing the mucus layer of the gastrointestinal tract of laboratory rodents. Int J Syst Evol Microbiol. 2005; 55(Pt 3):1199–204. https://doi.org/10.1099/ijs.0.63472-0 PMID: 15879255

55. Li RW, Wu S, Li W, Navarro K, Couch RD, Hill D, et al. Alterations in the porcine colon microbiota induced by the gastrointestinal nematode Trichuris suis. Infect Immun. 2012; 80(6):2150–7. https://doi.org/10.1128/IAI.00141-12 PMID: 22493085

56. Ginsburg I. The role of bacteriolysis in the pathophysiology of inflammation, infection and post-infectious sequelae. APMIS. 2002; 110(11):753–70. PMID: 12588416

57. Brenchley JM, Douek DC. Microbial translocation across the GI tract. Annu Rev Immunol. 2012; 30:149–73. https://doi.org/10.1146/annurev-immunol-020711-075001 PMID: 22224779

58. Chassaing B, Etienne-Mesmin L, Gewirtz AT. Microbiota-liver axis in hepatic disease. Hepatology. 2014; 59(1):328–39. https://doi.org/10.1002/hep.26494 PMID: 23703735

59. Macpherson AJ, Heikenwalder M, Ganal-Vonarburg SC. The Liver at the Nexus of Host-Microbial Interactions. Cell Host Microbe. 2016; 20(5):561–71. https://doi.org/10.1016/j.chom.2016.10.016 PMID: 27832587

60. van der Poll T, Opal SM. Host-pathogen interactions in sepsis. Lancet Infect Dis. 2008; 8(1):32–43. https://doi.org/10.1016/S1473-3099(07)70265-7 PMID: 18063412

61. George PJ, Anuradha R, Kumar NP, Kumaraswami V, Nutman TB, Babu S. Evidence of microbial translocation associated with perturbations in T cell and antigen-presenting cell homeostasis in hookworm infections. PLoS neglected tropical diseases. 2012; 6(10):e1830. https://doi.org/10.1371/journal.pntd.0001830 PMID: 23056659

62. Brenchley JM, Price DA, Schacker TW, Asher TE, Silvestri G, Rao S, et al. Microbial translocation is a cause of systemic immune activation in chronic HIV infection. Nat Med. 2006; 12(12):1365–71. https://doi.org/10.1038/nm1511 PMID: 17115046

63. Caradonna L, Amati L, Lella P, Jirillo E, Caccavo D. Phagocytosis, killing, lymphocyte-mediated antibacterial activity, serum autoantibodies, and plasma endotoxins in inflammatory bowel disease. Am J Gastroenterol. 2000; 95(6):1495–502. https://doi.org/10.1111/j.1572-0241.2000.02085.x PMID: 10894586

64. Caradonna L, Amati L, Magrone T, Pellegrino NM, Jirillo E, Caccavo D. Enteric bacteria, lipopolysaccharides and related cytokines in inflammatory bowel disease: biological and clinical significance. J Endotoxin Res. 2000; 6(3):205–14. PMID: 11052175

65. Gardiner KR, Halliday MI, Barclay GR, Milne L, Brown D, Stephens S, et al. Significance of systemic endotoxaemia in inflammatory bowel disease. Gut. 1995; 36(6):897–901. PMID: 7615280

66. Rosenthal P. Assessing liver function and hyperbilirubinemia in the newborn. National Academy of Clinical Biochemistry. Clin Chem. 1997; 43(1):228–34. PMID: 8990258

67. Giannini EG, Testa R, Savarino V. Liver enzyme alteration: a guide for clinicians. CMAJ. 2005; 172(3):367–79. https://doi.org/10.1503/cmaj.1040752 PMID: 15684121

68. DeRubertis FR, Woeber KA. Accelerated cellular uptake and metabolism of L-thyroxine during acute Salmonella typhimurium sepsis. J Clin Invest. 1973; 52(1):78–87. https://doi.org/10.1172/JCI107176 PMID: 4629910

69. Malik R, Hodgson H. The relationship between the thyroid gland and the liver. QJM. 2002; 95(9):559–69. PMID: 12205333

70. Wartofsky L. The response of the thyroid gland and thyroid hormone metabolism to infectious disease. Horm Res. 1974; 5(2):112–28. https://doi.org/10.1159/000178623 PMID: 4130024

71. Kamath PS. Clinical approach to the patient with abnormal liver test results. Mayo Clin Proc. 1996; 71(11):1089–94; quiz 94–5. https://doi.org/10.1016/S0025-6196(11)63282-5 PMID: 8917295

72. van der Spek AH, Fliers E, Boelen A. Thyroid hormone metabolism in innate immune cells. J Endocrinol. 2017; 232(2):R67–R81. https://doi.org/10.1530/JOE-16-0462 PMID: 27852725

73. Cassat JE, Skaar EP. Iron in infection and immunity. Cell Host Microbe. 2013; 13(5):509–19. https://doi.org/10.1016/j.chom.2013.04.010 PMID: 23684303

74. Northrop-Clewes CA. Interpreting indicators of iron status during an acute phase response—lessons from malaria and human immunodeficiency virus. Ann Clin Biochem. 2008; 45(Pt 1):18–32. https://doi.org/10.1258/acb.2007.007167 PMID: 18275670

75. Schreiber F, Arasteh JM, Lawley TD. Pathogen Resistance Mediated by IL-22 Signaling at the Epithelial-Microbiota Interface. J Mol Biol. 2015; 427(23):3676–82. https://doi.org/10.1016/j.jmb.2015.10.013 PMID: 26497621

76. Broadhurst MJ, Leung JM, Kashyap V, McCune JM, Mahadevan U, McKerrow JH, et al. IL-22+ CD4+ T cells are associated with therapeutic trichuris trichiura infection in an ulcerative colitis patient. Sci Transl Med. 2010; 2(60):60ra88.

77. Leung JM, Loke P. A role for IL-22 in the relationship between intestinal helminths, gut microbiota and mucosal immunity. Int J Parasitol. 2013; 43(3–4):253–7. https://doi.org/10.1016/j.ijpara.2012.10.015 PMID: 23178750

78. Marillier RG, Michels C, Smith EM, Fick LC, Leeto M, Dewals B, et al. IL-4/IL-13 independent goblet cell hyperplasia in experimental helminth infections. BMC Immunol. 2008; 9:11. https://doi.org/10.1186/1471-2172-9-11 PMID: 18373844

79. Reyes JL, Fernando MR, Lopes F, Leung G, Mancini NL, Matisz CE, et al. IL-22 Restrains Tapeworm-Mediated Protection against Experimental Colitis via Regulation of IL-25 Expression. PLoS Pathog. 2016; 12(4):e1005481. https://doi.org/10.1371/journal.ppat.1005481 PMID: 27055194

80. Chiriac MT, Buchen B, Wandersee A, Hundorfean G, Gunther C, Bourjau Y, et al. Activation of Epithelial Signal Transducer and Activator of Transcription 1 by Interleukin 28 Controls Mucosal Healing in Mice With Colitis and Is Increased in Mucosa of Patients With Inflammatory Bowel Disease. Gastroenterology. 2017; 153(1):123–38 e8. https://doi.org/10.1053/j.gastro.2017.03.015 PMID: 28342759

81. Mansfield LS, Urban JF Jr. The pathogenesis of necrotic proliferative colitis in swine is linked to whipworm induced suppression of mucosal immunity to resident bacteria. Vet Immunol Immunopathol. 1996; 50(1–2):1–17. PMID: 9157675

82. Stephenson LS, Holland CV, Cooper ES. The public health significance of Trichuris trichiura. Parasitology. 2000; 121 Suppl:S73–95.

83. MacDonald TT, Spencer J, Murch SH, Choy MY, Venugopal S, Bundy DA, et al. Immunoepidemiology of intestinal helminthic infections. 3. Mucosal macrophages and cytokine production in the colon of children with Trichuris trichiura dysentery. Trans R Soc Trop Med Hyg. 1994; 88(3):265–8. PMID: 7974659

84. Figueiredo CA, Barreto ML, Alcantara-Neves NM, Rodrigues LC, Cooper PJ, Cruz AA, et al. Coassociations between IL10 polymorphisms, IL-10 production, helminth infection, and asthma/wheeze in an urban tropical population in Brazil. J Allergy Clin Immunol. 2013; 131(6):1683–90. https://doi.org/10.1016/j.jaci.2012.10.043 PMID: 23273955